Atmospheric Research 315 (2025) 107864

Contents lists available at ScienceDirect

Atmospheric Research

journal homepage: www.elsevier.com/locate/atmosres

Aerosol optical depth over Northeastern Brazil: A multi-platform intercomparison study

Gabriel Bonow Münchow[a,b,*], Aline Macedo de Oliveira[c], Ediclê De Souza Fernandes Duarte[d,e], Daniel Camilo Fortunato dos Santos Oliveira[f], Bárbara Marinho Araujo[a], Nilton Manuel Évora do Rosário[g], Judith Johanna Hoelzemann[h,**]

[a] Graduate Program in Climate Sciences, Federal University of Rio Grande do Norte, Av. Senador Salgado Filho, 3000, 59078-970 Natal/RN, Brazil
[b] State Research Center for Remote Sensing and Meteorology, Federal University of Rio Grande do Sul, Av. Bento Gonçalves, 9500, 91501-900, Porto Alegre/RS, Brazil
[c] Federal University of Rio Grande do Norte, Av. Senador Salgado Filho, 3000, 59078-970, Natal/RN, Brazil
[d] Instituto de Ciências da Terra – ICT (Pólo de Évora), Instituto de Investigação e Formação Avançada (IIFA), Universidade de Évora, 7000-671 Évora, Portugal
[e] Department of Physics, School of Sciences and Technology, University of Évora, Évora, Portugal
[f] CommSensLab, Department of Signal Theory and Communication, Universitat Politècnica de Catalunya, Carrer de Jordi Girona, 31, 08034 Barcelona, Spain
[g] Department of Environmental Sciences, Federal University of São Paulo, Rua São Nicolau, 210, 09913-030, Diadema/SP, Brazil
[h] Department of Atmospheric and Climate Sciences, Federal University of Rio Grande do Norte, Av. Senador Salgado Filho, 3000, 59078-970 Natal/RN, Brazil

ARTICLE INFO

Keywords:
AOD
MODIS
MERRA2
Brazilian Biomes
Brazilian Northeast

ABSTRACT

The atmosphere over the Northeastern region of Brazil (NEB) contains a variety of different aerosol types: marine, soil dust, biomass burning, urban pollution, as well as mixed species. However, very few reliable information on aerosols is available for the region. Satellite data provides spatial and temporal coverage in places with low density ground-based observational networks, with Aerosol Optical Depth (AOD) products as most important information on the atmospheric aerosol load. To find out how different AOD products from satellites behave over the NEB region we compared AOD at 550 nm from MODIS retrievals aboard both NASA's Terra and Aqua satellites, and ground-based derived AOD 550 nm from the two Aerosol Robotic Network (AERONET) sites in the region, located in cities of Petrolina and Natal, between 2015 and 2018. We based our analysis on the following MODIS AOD retrievals products: Dark Target (DT), Deep Blue (DB), the combined product (DTDB), DT 3 km resolution product (MxD3k) and MAIAC at 1 km resolution. Additionally, we used AOD from MERRA2 reanalysis for another comparison that may provide additional insight on which products perform best over the region. We also analyze and compare the seasonality of the AOD products to the four biomes of NEB, which are Amazon rainforest, Atlantic Forest, Cerrado and Caatinga (wooded savannah-like) biomes. Petrolina is located in the NEB largest biome, the Caatinga, while Natal is a coastal city in the Atlantic Forest. The results show that DB yields the best results for the Petrolina site. The analyses also show that in all biomes the AOD monthly averages decrease during austral autumn and winter and increase during spring and summer. The compared products show some differences in AOD, even though with similar patterns. MAIAC and DB show very similar values in all four biomes throughout the year, recommending the use of DB and MAIAC for studies in the Caatinga region.

1. Introduction

The role of aerosols in the atmosphere has been studied for decades, from the global climate change scale, altering the earth's radiative budget and the hydrological cycle (Albrecht, 1989; Altaratz et al., 2014; Arias et al., 2021; Kaufman and Koren, 2006a, 2006b; Koren et al., 2008; Twomey, 1977) to the local air quality scale (Ignotti et al., 2010; Marlier et al., 2020; Martins et al., 2018; Millman et al., 2008), especially in

* Corresponding author at: Graduate Program in Climate Sciences, Federal University of Rio Grande do Norte, Av. Senador Salgado Filho, 3000, 59078-970 Natal/RN, Brazil.
** Corresponding author.
E-mail addresses: gabrielbm@ufrgs.br (G.B. Münchow), oliveiraamacedo@gmail.com (A.M. de Oliveira), edicle.duarte@uevora.pt (E.D.S.F. Duarte), daniel.camilo.fortunato@upc.edu (D.C.F.S. Oliveira), mbarbaraengamb@gmail.com (B.M. Araujo), nrosario@unifesp.br (N.M.É. Rosário), judith.hoelzemann@ufrn.br (J.J. Hoelzemann).

https://doi.org/10.1016/j.atmosres.2024.107864
Received 24 June 2024; Received in revised form 6 December 2024; Accepted 6 December 2024
Available online 9 December 2024

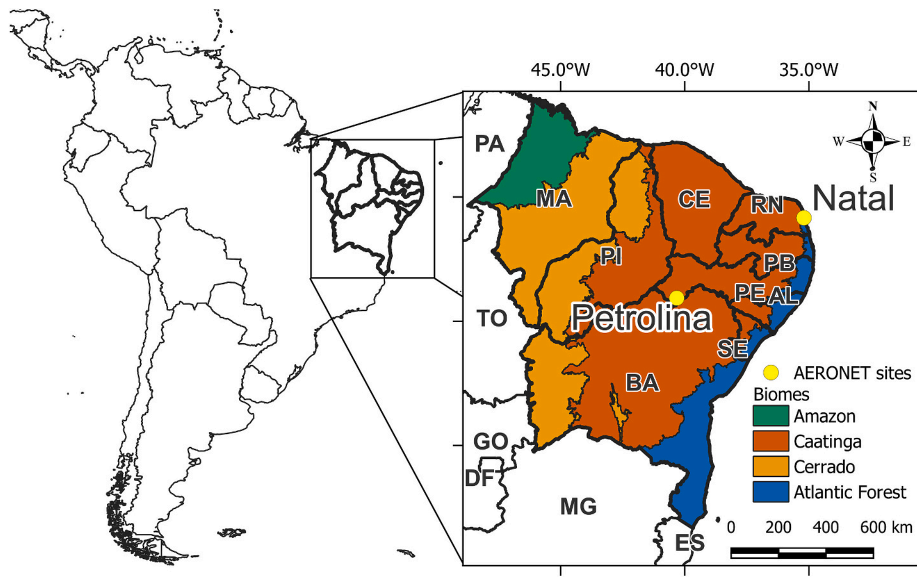

Fig. 1. Area of the Northeastern Brazil (NEB). Shaded colors are used to describe NEB's biomes. Yellow dots are the locations of the AERONET operating sites in the cities of Petrolina/PE and Natal/RN. (For interpretation of the references to colour in this figure legend, the reader is referred to the web version of this article.)

major urban areas (Alpopi and Colesca, 2010; de Andrade et al., 2017; Molina and Molina, 2004; Parrish et al., 2011). Atmospheric aerosols present a high variability in their temporal, spatial and physio-chemical properties. The anthropogenic aerosols that mainly contribute to climate change are sulfur dioxide, organic carbon, ammonia and black carbon. The quantitative contribution of these aerosols to global climate until today present the highest source of uncertainty in the global radiative forcing budget (Arias et al., 2021).

The atmosphere over Northeastern Brazil (NEB) contains a variety of aerosol types: marine, soil dust from regional and remote sources (Sahara desert) and smoke, mainly from local biomass burning but also transported across the Atlantic from the sub-sahel region, further urban pollution, and mixed species (Landulfo et al., 2016; dos Oliveira et al., 2021; de Oliveira et al., 2019; de Oliveira-Júnior et al., 2022). However, there is a lack of reliable information on the aerosol amount, properties, and impacts in the NEB region. There are only fifteen surface air quality monitoring stations in the entire NEB domain, which enclose an area of 1,558,000 km^2, ten of them located in only one state (Bahia), four in Pernambuco and one in Ceará (Ferreira et al., 2022). However, most of the sites do not provide new data since the last years. Satellite data generally provide spatial and temporal coverage of atmospheric composition information across the entire world including the NEB, providing a crucial option to regions with low density or non-existent observational networks. A key parameter used in the monitoring of atmospheric composition by satellites is the Aerosol Optical Depth (AOD), which measures the extinction of electromagnetic radiation due to interaction with aerosols, from the surface to the top of the atmosphere at specific spectral bands. The AOD is a quantitative estimate of aerosol amount in the atmosphere, and can be used as a proxy for surface particulate matter. Assessment of satellite-based AOD over the NEB can be an important source of information to mitigate the lack of in situ measurements. The AOD datasets have been produced from both surface remote sensing platforms, such as the Aerosol Robotic Network (AERONET) (Holben et al., 1998), and from satellites sensors such as the Advanced Very-High-Resolution Radiometer - AVHRR (Zhao et al., 2008), Sea-viewing Wide Field-of-view Sensor - SeaWiFS (Sayer et al., 2012), Moderate Resolution Imaging Spectroradiometer - MODIS (Levy et al., 2013), Multi-angle Imaging SpectroRadiometer - MISR (Witek et al., 2013) and also the Visible Infrared Imaging Radiometer Suite - VIIRS (Hsu et al., 2019; Sayer et al., 2018). However, the variability of AOD values between the different available products has been a matter of concern, especially regarding the differences in magnitude and temporal tendencies. Satellite AOD retrievals are expected to be influenced by uncertainties associated with the assumptions of the aerosol model that represent aerosol properties, the effect of the correction of surface reflectance, cloud contamination, and radiometric calibration (Li et al., 2009).

Considering the number of AOD products available, there is a need to evaluate and validate these over the region of interest. There are some efforts to evaluate and find the best AOD product in different scenarios. Jiang et al. (2023) compared the MODIS AOD using Dark Target (DT), Deep Blue (DB), and Multi-Angle Implementation Atmospheric Correction (MAIAC) over China and found that MAIAC had more matches and accuracy when compared with AERONET data and data from the Sun–Sky Radiometer Observation Network (SONET). Considering all databases, the authors found that Root Mean Squared Error (RMSE), Bias, R^2, and data within the Expected Error (EE) were 0.243, 0.151, 0.745, and 41.43 %, respectively, using DT products only, and 0.174, 0.027, 0.761, and 56.98 % using the DB algorithm-based products and 0.197, 0.036, 0.722 and 65.64 % for MAIAC data. They also show that MAIAC presents its lowest accuracy over water and higher accuracy over forests, cropland, and mixed land cover types. Similar results were found by Jethva et al. (2019), who also compared these 3 algorithms with AERONET over North America. They found that over dark surfaces, the performance of all three algorithms is similar, with MAIAC showing a slightly better result. The RMSE and correlation were 0.056 and 0.900 for MAIAC, respectively, 0.095 and 0.933 for DT, and 0.069 and 0.756 for DB. Over bright surface background and mountainous regions, both MAIAC and DB showed a good agreement with AERONET data, with an RMSE of ~0.06 and correlation of 0.830 and 0.720, respectively, while DT overestimated the AOD, an RMSE of 0.120, correlation of 0.820 and bias of 0.037. The authors also highlighted the higher number of matchups with AERONET of MAIAC, when compared with DT and DB. Choi et al. (2019) showed an AOD comparison from multi-satellite AOD against AERONET over East Asia and found that MAIAC and MISR showed a higher correlation, with 0.93, and a RMSE of 0.15 and 0.12, respectively. The MODIS DT and VIIRS yielded the lowest correlation, with 0.870, and a RMSE of 0.220 and 0.160. Nguyen et al. (2019) found a correlation of 0.81 and 0.68 between AERONET against MODIS DT and VIIRS, respectively, in the Southeast Asia region. On a global scale, Chen et al. (2022) showed that MODIS DT presents the lowest correlation (r), with 0.820, while VIIRS DB has the highest one, with 0.866. Martins

Table 1
Monthly and annual precipitation (mean ± standard deviation) for the NEB biomes, between 1979 and 2013 based on the CHELSA database. Bold numbers reflect the three months of highest precipitation for each biome.

Precipitation Seasonality in the NEB Biomes (mm)				
	AMAZON	ATLANTIC FOREST	CERRADO	CAATINGA
Jan	234 ± 100	88 ± 56	**198.9 ± 98**	102 ± 76
Feb	**282 ± 106**	98 ± 60	**189.6 ± 76**	**111 ± 55**
Mar	**371 ± 86**	130 ± 59	**203.1 ± 63**	**143 ± 65**
Apr	**340 ± 132**	**155 ± 63**	142.0 ± 66	**119 ± 63**
May	197 ± 87	**147 ± 42**	57.7 ± 37	61 ± 35
Jun	99 ± 46	**157 ± 50**	15.9 ± 9	41 ± 21
Jul	66 ± 31	138 ± 36	9.3 ± 7	29 ± 11
Aug	32 ± 16	102 ± 31	7.3 ± 7	18 ± 7
Sep	29 ± 14	71 ± 28	20.3 ± 15	13 ± 7
Oct	36.3 ± 22.3	77.6 ± 30.7	65.3 ± 35	22 ± 15
Nov	56.9 ± 27.7	103.1 ± 44.1	124.8 ± 43	48 ± 24
Dec	111.6 ± 54.7	99.8 ± 61.1	169.9 ± 65	69 ± 48
Annual	1848 ± 419	1364 ± 217	1197 ± 219	773 ± 212

Adapted from Correia Filho et al. (2019).

et al. (2017) validated MAIAC aerosol product over South America, comparing with AERONET AOD data, and found a correlation coefficient of 0.956 to Terra and 0.949 to Aqua. However, in their analysis, there were no AERONET sites in the NEB. More recently, Rudke et al. (2023) evaluated AOD MODIS products DT, DB, MAIAC, and the DT 3 km, over Brazil and concluded that MAIAC and DB yields smaller error and uncertainties than DT. Nevertheless, the DT shows better results over forested areas. In the Savanna region, the study results show a RMSE between 0.038 (Aqua DB) and 0.108 (Terra DT 3Km) and a correlation coefficient between 0.71 (Aqua DB) and 0.46 (Aqua MAIAC).

To determine the quality of AOD products from MODIS in more detail for the Northeastern Brazilian region, this paper evaluates and validates the AOD of distinct MODIS products, including all AERONET stations available in the region, and also analyzing their performance according to the different biomes. We compare the DB, DT, and MAIAC products based on MODIS retrievals, located aboard Terra and Aqua satellites. As AOD reference we used the AOD from the AERONET network stations within the region. We also included the AOD from Modern-Era Retrospective Analysis for Research and Applications, Version 2 (MERRA2) in the intercomparison. Section 2 of the paper describes and characterizes the region of NEB and the database used. Section 3 shows the AOD products collocation strategy, the data analysis methodology, the results of MODIS products validation against AERONET, as well as a regional analysis by the different biomes. Finally, in section 4 we present our conclusions.

2. Description of region, dataset, and methodology

2.1. The region of Northeast Brazil

The Northeastern region of Brazil (NEB) is located in tropical latitudes, with 1,552,175 km^2 of area, which is approximately 18 % of the total Brazilian territory, and almost three times the size of France. It is the second most populated region of Brazil, with ~54.6 million inhabitants (IBGE, 2023). This population is concentrated mostly along the coastal areas, where most of the NEB state capitals are located. There are nine States in NEB (Fig. 1): Alagoas (AL), Bahia (BA), Ceará (CE), Maranhão (MA), Paraíba (PB), Piauí (PI), Pernambuco (PE), Rio Grande do Norte (RN) and Sergipe (SE). The NEB is composed of four distinct biomes in the NEB, namely Amazon Rainforest (7.3 % of NEB area), Atlantic Forest (10.0 %), Cerrado (29.2 %), and Caatinga (53.5 %) (IBGE, 2019).

The climate of NEB is affected by multi-scale processes. At the global scale systems and phenomena such as the El Niño-Southern Oscillation (ENSO), North Atlantic Oscillation (NAO), South Atlantic Subtropical Anticyclone (SASA), North Atlantic Subtropical Anticyclone (NASA), and the Intertropical Convergence Zone (ITCZ) play an important role. At mesoscale, for instance, there are influences of Mesoscale Complex systems, Squall Lines and, very rarely, frontal systems. At the synoptic scale one of the most famous elements of the NEB climatology is the Upper Level Cyclonic Vortex (ULCV) (de Cavalcanti et al., 2009; dos Reis et al., 2021; Kodama, 1992; Kousky, 1980, 1979; Kousky and Gan, 1981; Uvo, 1989). The raining season in the Amazon, Cerrado and Caatinga biomes in the NEB, takes place between January and April, while in the Atlantic Forest it occurs from March to July (Table 1). The dry season occurs between August and October in the Amazon, Caatinga, and Atlantic Forest, and between June and August in Cerrado (Correia Filho et al., 2019; Oliveira et al., 2017). In the NEB region, the wind origins mainly from east and southeast, varying from northeast in the Amazon region of the state of Maranhão, to southeast in the center of Bahia and the coast of Rio Grande do Norte, Pernambuco, and Paraiba states (de INMET, 2018). The mean annual temperature ranges between 20° and 28 °C, except for a few elevated regions where mean temperatures of lower than 20 °C may prevail (Kayanoi and Andreoli, 2009).

The NEB atmosphere has been characterized as containing a small load of atmospheric aerosols, mainly when compared with the biomass-burning regions of the Amazon basin and center-west of Brazil (do Rosário et al., 2022; Rosário et al., 2013). de Oliveira et al. (2019) showed that the AOD average at 550 nm, across the NEB biomes is 0.20, ranging from 0.04 to 0.52. The authors also showed that there are two periods during the year when AOD values are more elevated, from January to March and from August to October. During the first period, the increase in AOD is either caused by advection of aerosols from dust storms in the Sahara or from carbonaceous aerosols from fires in the sub-sahel region of northern hemispheric Africa, while during the second period the increase is caused by the advection of marine aerosols from the coast due to the higher wind intensity during that period, and occasionally due to the transportation of fire smoke plumes from fires in the African equatorial tropical forest (Landulfo et al., 2016; de Oliveira et al., 2019).

The Amazon biome is a tropical forest composed mostly of Evergreen Forest, wetlands, and water bodies, with some savanna and natural grassland. The predominant land use is agriculture, cattle ranching, mining, logging, and non-timber forestry production. The Caatinga is composed of woody and deciduous forests. The region is used for agriculture, cattle ranching, smallholder livestock production, non-timber forestry, and urbanization. The biome Cerrado is composed of savannas, grasslands, and forests, where the predominant land use is agriculture, cattle ranching, timber exploitation for coal production, and artificial water reservoirs. The Atlantic Forest has isolated forest fragments, mostly old secondary growth, forest plantation, croplands, pasture, urbanized areas and infrastructure. Six of the nine state capitals in Northeastern Brazil are located in the Atlantic Forest biome (Souza et al., 2020). Due to this variety of land use and cover the surface reflectance across the NEB shows different patterns according to region.

2.2. AERONET

The Aerosol Robotic Network (AERONET) is a global project that characterizes aerosol optical properties worldwide using ground-based remote sensing (Giles et al., 2019; Holben et al., 1998). The Cimel Sun-Photometers are able to measure spectral Sun direct irradiance and sky radiances between the channels 340 nm to 1640 nm. AERONET provides AOD, other optical properties, as well as microphysical properties for three data quality levels: Level 1.0 (unscreened), Level 1.5 (near-real-time automatic cloud screening and automatic instrument anomaly quality control) and Level 2.0 (level 1.5 with pre-field and post-field calibrations). Inversions of precipitable water and other AOD-dependent products are derived from these levels and may implement additional quality checks. The AOD estimated uncertainty is ~0.010–0.021, due primarily to instrument calibration. The errors depend on the wavelength, with higher values in the UV. AOD accuracy

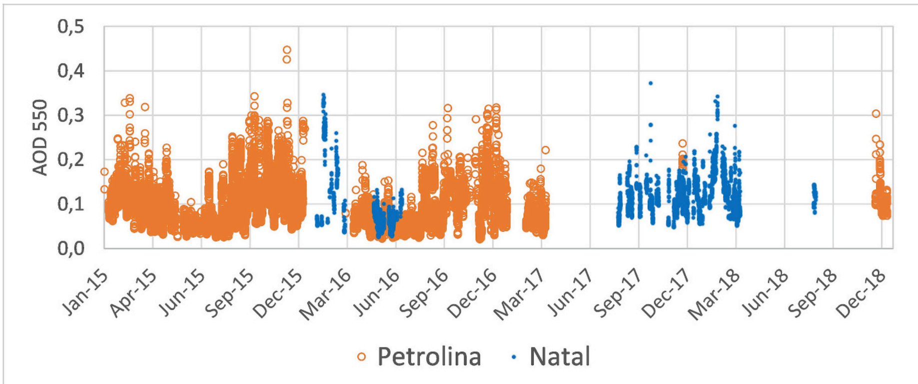

Fig. 2. Database of AOD 550 nm from AERONET sites at Petrolina-PE and Natal-RN, Brazil.

also depends on the uncertainties in the estimations of the optical air mass, optical depths of Rayleigh and ozone, and the column water vapor (Dubovik and King, 2000; Eck et al., 1999; Holben et al., 1998; Sinyuk et al., 2020). The NEB region only has two sites to monitor atmospheric aerosols on an operational basis, one at Petrolina-PE and the other at Natal-RN (Fig. 1). Petrolina is located at 9.069°S; 40.320°W, in the western region of Pernambuco state. It is located in a semi-arid region, within the Caatinga biome. It is the only city with a consolidated AERONET long-term monitoring in NEB, with observations from 2004 until today. Natal, located at 5.84157°S; 35.19965°W, is a coastal city in the Rio Grande do Norte state, within the Atlantic Forest biome. In Natal, the measurements started in 2016, with irregular observations from Jan/2016 to Jul/2016 and Aug/2017 to Mar/2018, and on Aug/2018. In this study, we use level 2.0 data from Version 3. For Petrolina we use Version 3 level 2.0 quality-assured data from 2015, Apr/2016 to Mar/2017, Dec/2017, and Nov/2018 to Dec/2018 (Fig. 2). We opted to analyze the MODIS AOD dataset to the years of 2015 to 2018 to obtain a recent continuous timeseries that encompasses the period available of the data from both sites. Besides these two sites from AERONET, there is no other ground-based operational observational data in the region retrieving AOD.

2.3. MODIS

The sensor MODerate resolution Imaging Spectroradiometer (MODIS), one of the first developed targeting AOD monitoring, is installed on board the Terra and Aqua sun-synchronous satellites, launched in 1999 and 2002, respectively. Terra overpasses the NEB region in the morning while Aqua overpasses during the afternoon. Both satellites cover the entire earth's surface every 1 to 2 days. MODIS is a passive spectroradiometer with 36 bands in the visible and thermal wavelengths and resolution of 250 m, 500 m, and 1 km at nadir, according to the band. MODIS products are classified into seven levels, where level-2 (L2) represents the derived geophysical variables from level-1 swath data with georeferenced information and atmospherically corrected. Level-2G is the L2 data mapped in a sinusoidal tiled gridded system (https://modis.gsfc.nasa.gov).

The MODIS aerosol products level-2 recent collection C061 MOD04_L2 (Terra) and MYD04_L2 (Aqua) provide AOD at wavelength 550 nm (AOD550), with 10 km of spatial resolution at nadir (Levy et al., 2015, 2013). An alternative product named MOD04_3k and MYD04_3k, provides AOD with 3 km of spatial resolution (Gupta et al., 2018; Remer et al., 2013). The MxD04_L2 products are retrieved based on 2 independent algorithms: Dark Target (DT) and Deep Blue (DB). Targeting MODIS AOD application to monitor aerosols at an intra-urban scale, the most recently available product is the Multi-Angle Implementation of Atmospheric Correction (MAIAC – MCD19A2) at 1 km spatial resolution (Lyapustin et al., 2018, 2011a, 2011b). MAIAC data is available in Level-2G.

After 2000, with the launch of the Terra satellite, with its MODIS sensor, the DT algorithm have been used to derive AOD. Two entirely independent DT algorithms are applied to calculate AOD over dark surfaces of the ocean (Levy et al., 2003; Tanre et al., 1997) and land (Kaufman et al., 1997), such as non-glint open ocean scene and dark vegetated landscape. The land algorithm uses the reflectance of MODIS channels 0.47 μm, 0.66 μm, and 2.13 μm. The EE to DT data over land from MxD04_L2 is $\pm(0.05 + 0.15\ \tau_A)$, where τ_A is the AOD observed by AERONET (Levy et al., 2010, 2013).

Due to the limitation of DT to retrieval AOD over bright surfaces, Hsu et al. (2004, 2006) have developed the DB algorithm to retrieve aerosol properties over deserts and bright land surfaces, except for ice and snow. For MODIS data, the algorithm uses channels 412 nm, 470 nm, and 650 nm. The aerosol characteristics are estimated by comparing the radiances measured by the satellite sensor with pre-calculated reflectances from look-up tables to find the best match (Sayer et al., 2013). Hsu et al. (2013) estimated an EE for the DB data over land from MxD04_L2 of $\pm(0.05 + 0.2\tau_A)$.

Since the C6 MODIS collection, the DB algorithm provides information on aerosol properties over vegetated land surfaces. For this reason, the C6 collection provides a merged product combining the DT and DB retrievals. To merge them, a monthly Difference Vegetation Index (NDVI) climatology over land was used. The DB data is used for Normalized NDVI $\leq$0.2 and the DT data for NDVI $\geq$0.3. If 0.2 $\leq$ NDVI $\leq$0.3 the product with a higher QA flag is used. If both products present a QA = 3, the mean value is used (Sayer et al., 2014).

The MODIS AOD not only is applied for climate studies but also for small-scale air quality studies (de Castanho et al., 2008; Li et al., 2005). For this reason, Remer et al. (2013) developed an AOD product with 3 km spatial resolution (MOD04_3k/MYD04_3k), available in the C6 MODIS collection. This product is similar to the 10 km product, also using the DT algorithm. The main difference is the quantity of pixels selected to retrieve AOD. While the 10 km product uses a retrieval box with 400 px (20 × 20 px) with 10 × 10 km, the MxD04_3k uses a retrieval box of 36 px (6 × 6 px) with 3 × 3 km spatial resolution. Both products filter the pixels for clouds, bright surfaces, snow, ice, ocean sediments, sun glint, and inland water. They also eliminate the brightest and darkest pixels (Gupta et al., 2018). Globally, over land, this product has an EE of $\pm(0.05 + 0.2\tau_A)$ (Remer et al., 2013).

The traditional DT (10 km) and the new DB products and 3 km algorithms are based on the instant measurement for each pixel in swath-based data. The Multi-Angle Implementation Atmospheric Correction (MAIAC - MCD19A2) algorithm interpolates the radiance measurements to a fixed 1 km horizontal grid. Using the sliding window technique, the algorithm accumulates 16 days of measurements from different orbits, creating a time series for each cell. It helps to separate the atmospheric and surface radiometric contributions as the same point is observed over

Table 2
MODIS aerosol products in the hdf data files.

SDS Name product / SDS Quality Flag	Expected Error (EE)	Exp name TERRA AQUA
Dark Target (DT)		
- Image_Optical_Depth_Land_And_Ocean	±(0.05 + 15 %)	MOD_DT MYD_DT
- Land_Ocean_Quality_Flag		
Deep Blue (DB)		
- Deep_Blue_Aerosol_Optical_Depth_550_Land	±(0.05 + 20 %)	MOD_DB MYD_DB
- Deep_Blue_Aerosol_Optical_Depth_550_Land_QA_Flag		
Combine Dark Target and Deep Blue (DTDB)		
- AOD_550_Dark_Target_Deep_Blue_Combined		MOD_DTDB MYD_DTDB
- AOD_550_Dark_Target_Deep_Blue_Combined_QA_Flag		
Dark Target (3 k)		
- Image_Optical_Depth_Land_And_Ocean	±(0.05 + 20 %)	MOD_3k MYD_3k
- Land_Ocean_Quality_Flag		
MAIAC		
- Optical_Depth_055	±(0.05 + 10 %)	MOD_MAIAC MYD_MAIAC
- AOD_QA		

Table 3
Number of pixels inside the 0.5° x 0.5° box centered and collocated with AERONET AOD data from Petrolina/PE with all valid values and only the best quality control flags for each AOD product and its respectively mean AOD.

Product	Pix Count		Mean AOD Valid pixels (All QA)	Mean AOD Best QA
	Valid (all QA)	Best QA		
MOD_DT	1627	820	0.016	−0.014
MOD_DB	2460	1509	0.120	0.093
MOD_DTDB	944	934	0.001	−0.002
MOD_3K	11,610	9965	0.026	0.025
MOD_MAIAC	320,109	252,787	0.146	0.123
MOD_3Ens_MEAN	–	96,363	–	0.057
MOD_3Ens_MEDIAN	–	96,363	–	0.078
MOD_4Ens_MEAN	–	96,363	–	0.041
MOD_4Ens_MEDIAN	–	96,363	–	0.032
MYD_DT	1153	499	0.009	−0.022
MYD_DB	2239	1153	0.100	0.060
MYD_DTDB	614	606	−0.010	−0.010
MYD_3k	7322	6264	0.010	0.007
MYD_MAIAC	465,146	351,316	0.153	0.124
MYD_3Ens_MEAN	–	80,487	–	0.033
MYD_3Ens_MEDIAN	–	80,487	–	0.050
MYD_4Ens_MEAN	–	53,476	–	0.016
MYD_4Ens_MEDIAN	–	53,476	–	0.008
MERRA2	–	3118	–	0.079

time with different angles (Lyapustin et al., 2012a, 2012b, 2011a, 2011b). MAIAC provides aerosol retrievals over bright and dark surfaces. Lyapustin et al. (2018) estimated a globally EE of $\pm(0.05 + 0.1\tau_A)$.

Due to the MODIS scan geometry with its swath width of ~2330 km, the MxD04 horizontal resolution of 10 × 10 km at nadir (viewing zenith angle 0°) degrades toward the swath edges (viewing zenith angle ~65°), increasing up to 20 × 40 km. In addition to this across-track distortion, there is also overlap between pixels in consecutive along-track scans. These effects are known as "bow-tie effect" (Barnes et al., 1998; Remer et al., 2020; Sayer et al., 2015a, 2015b; Wolfe et al., 1998). This results in AOD errors and uncertainties in the MxD04 products being dependent on the viewing zenith angle. The MAIAC product is also affected by this problem, but minimizes its impact by using a gridding algorithm based on scan-by-scan processing and area-weighted gridding method (Lyapustin et al., 2018; Wang and Lyapustin, 2007).

Table 2 summarize MODIS AOD product names in the hdf-files used in this paper, with their respective quality flags and the name of each product that is used from now on. We will use MOD to refer to Terra products, MYD to Aqua's, and MxD as either MOD or MYD.

In this study, we have developed a new approach to work with MODIS AOD products that consist of an ensemble of sensor products, combining the DT and DB, from MxD04_L2, MxD04_3k, and MAIAC. We performed four tests calculating the mean and the median of MxD_DT, MxD_DB, and MAIAC, named MxD_3EnsMean and MxD_3EnsMedian, testing the three algorithms with distinct processing methodology. In another ensemble we additionally include MxD_3k, named MxD_4EnsMean and MxD_4EnsMedian.

2.4. MERRA2

The Modern-Era Retrospective Analysis for Research and Applications, Version 2 (MERRA2) is an atmospheric reanalysis produced by Global Modeling and Assimilation Office, from North American National Aeronautics and Space Administration (GMAO / NASA). It uses the Goddard Earth Observing System, version 5 (GEOS-5) atmospheric model and a Gridpoint Statistical Interpolation (GSI) analysis scheme, with a three-dimensional variational approach (3DVAR). It provides data with 0.5° x 0.625° of spatial resolution, since 1980, of 1-hourly and 3-hourly instantaneous diagnostics, and time-averaged collections contain hourly, three-hourly, monthly, or monthly diurnal means. The set of assimilation input observations includes surface conventional data, ground-based remotely sensed, satellite-derived data, satellite retrievals, radio occultation, and satellite radiance (Gelaro et al., 2017). This version 2 of MERRA2 includes aerosols information, using a radiatively coupled version of the Goddard Chemistry, Aerosol, Radiation, and Transport model (GOCART) with the Goddard Aerosol Assimilation System (GAAS). The data assimilated is the bias-corrected AOD derived from AVHRR radiances (during the period of 1980 to 2002) and from MODIS radiances (Terra: 2000 onwards, Aqua: 2002 onwards), the AOD retrievals over bright land surfaces from MISR (2000–2014), and AOD level 2 from AERONET (1999–2014). The MODIS Dark Target radiances are assimilated over the land and ocean (Buchard et al., 2017; Randles et al., 2017). In this paper, the MERRA2 product used is the AOD hourly time-averaged collection from tavg1_2d_aer_Nx (M2T1NXAER) to compare with AERONET data (session 3.1). The regional analyses (section 3.2) used the AOD three-hourly instantaneous collection from inst3_2d_gas_Nx (or M2I3NXGAS). To compare this data with the Terra and Aqua retrievals, we used the output of 12 UTC and 15 UTC, respectively. These are the closest output times to the satellite's overpasses in the NEB region. Reanalysis products were useful to fill spatio-temporal gaps in the observation time series, as gaps are a common feature in AOD retrievals due to cloud coverage or the lack of adequate monitoring coverage.

2.5. Data analysis

For the collocated analysis, AOD data from AERONET ($\tau_{AERONET}$) was

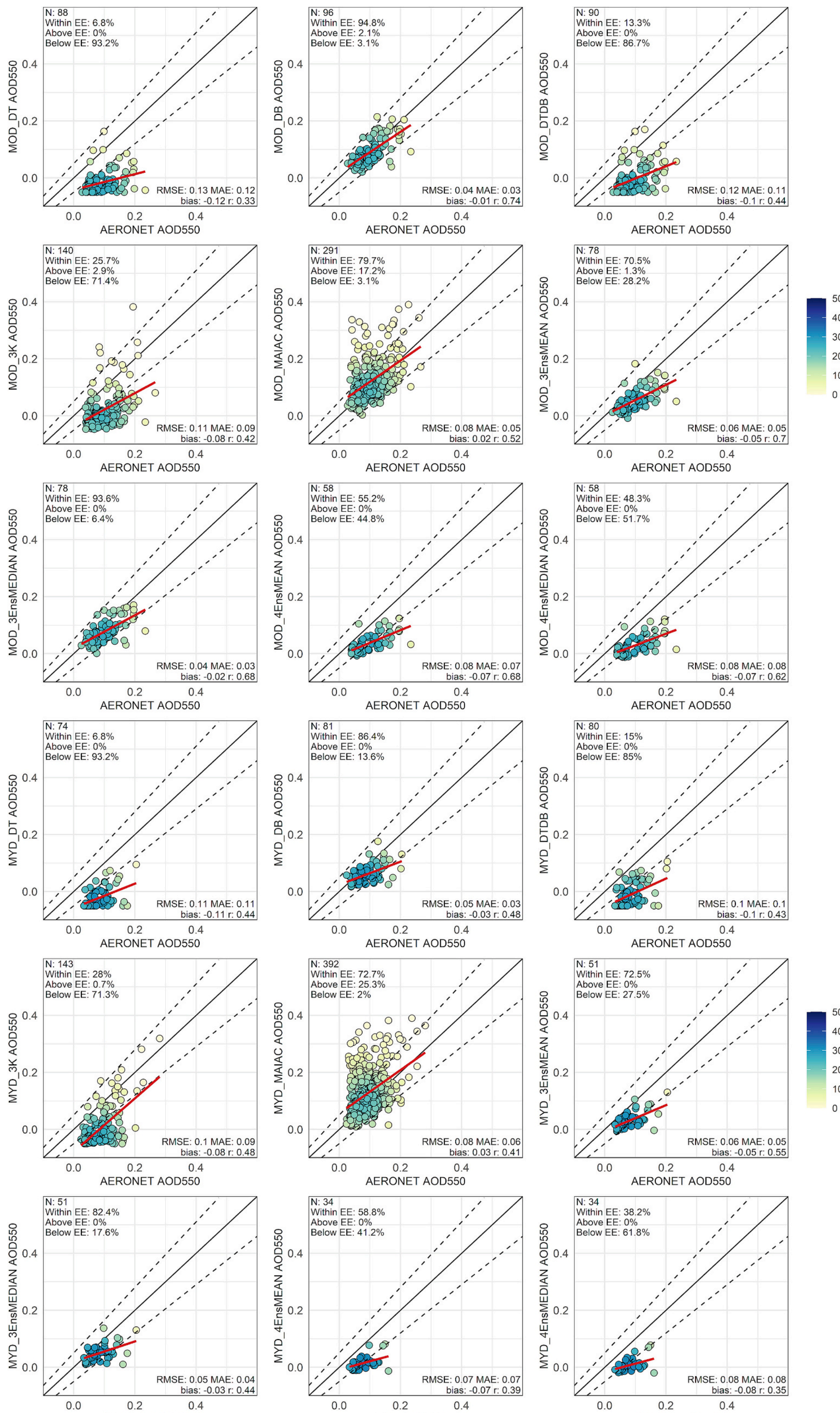

Fig. 3. Scatterplot of AOD550 from Aqua and Terra MODIS C6.1 Dark Target 10 km (DT), Deep Blue (DB), DTDB, Dark Target 3 km (3 k), MAIAC, and the ensemble products 3EnsMEAN, 3EnsMEDIAN, 4EnsMEAN and 4EnsMEDIAN as a function of AERONET AOD measurements over Petrolina/PE. The black solid line is the 1:1 line. The dashed lines are the expected error (EE) interval. N is the sample size, EE is the percentage of the samples within (=EE), under(<EE) or above (>EE) the expected error interval. (For interpretation of the references to colour in this figure legend, the reader is referred to the web version of this article.)

Table 4
Statistics of the comparison between AERONET AOD550 measurements and MODIS C6.1, from Terra (MOD) and Aqua (MYD), Dark Target 10 km (DT), Deep Blue (DB), DTDB, Dark Target 3 km (3 k), MAIAC AOD products, the ensemble products 3EnsMEAN, 3EnsMEDIAN, 4EnsMEAN, 4EnsMEDIAN, and MERRA2 over Petrolina/PE. EE is the percentage of the samples within (EE), under(<EE) or above (>EE) the expected error interval, sample size (N), RMSE, MAE, bias, and Spearman correlation (r) with 95 % CI. Darker colour indicates the best result of each index.

Product	Statistics							
	N	<EE	EE	>EE	RMSE	MAE	bias	r
MOD_DT	88	93	7	0	0.13	0.12	-0.12	0.33
MOD_DB	96	3	95	2	0.04	0.03	-0.01	0.74
MOD_DTDB	90	87	13	0	0.12	0.11	-0.10	0.44
MOD_3K	140	71	26	3	0.11	0.09	-0.08	0.42
MOD_MAIAC	291	3	80	17	0.08	0.05	0.02	0.52
MOD_3EnsMEAN	78	28	71	1	0.06	0.05	-0.05	0.70
MOD_3EnsMEDIAN	78	6	94	0	0.04	0.03	-0.02	0.68
MOD_4EnsMEAN	58	45	55	0	0.08	0.07	-0.07	0.68
MOD_4EnsMEDIAN	58	52	48	0	0.08	0.08	-0.07	0.62
MYD_DT	74	93	7	0	0.11	0.11	-0.11	0.44
MYD_DB	81	14	86	0	0.05	0.03	-0.03	0.48
MYD_DTDB	80	85	15	0	0.10	0.10	-0.10	0.43
MYD_3K	143	71	28	1	0.10	0.09	-0.08	0.48
MYD_MAIAC	392	2	73	25	0.08	0.06	0.03	0.41
MYD_3EnsMEAN	51	27	73	0	0.06	0.05	-0.05	0.55
MYD_3EnsMEDIAN	51	18	82	0	0.05	0.04	-0.03	0.44
MYD_4EnsMEAN	34	41	59	0	0.07	0.07	-0.07	0.39
MYD_4EnsMEDIAN	34	62	38	0	0.08	0.08	-0.08	0.35
MERRA2	3118	7	92	1	0.04	0.03	-0.02	0.75

interpolated to 550 nm using the Ångström exponent based on the 440 and 675 nm channels (da Lopes, 2011), since all AOD MODIS (τ_M) products are available only at 550 nm. The $\tau_{AERONET}$ was averaged using an interval of 1 h centered at the time of the satellite overpass. The MODIS AOD data was averaged across a box with 0.5° x 0.5° resolution centered at the surface sites (Remer et al., 2020). This is close to the 50 × 50 km box in the region of this study.

To perform an intercomparing analysis, we used the scatterplots with the percentage of the data falling within the expected error (EE), above (>EE) and under (<EE) of the $\pm(0.05 + 0.15\tau)$ envelope (Gupta et al., 2018; Levy et al., 2013). Although the products have different EE, the statistics using the same EE allows the products to be directly compared (Sayer et al., 2014). Additionally, error indexes (RMSE, MAE, and bias) and Spearman Rank correlation coefficient (r) were added to the analysis. We adopted the Spearman correlation due the small data sample in Natal site. This coefficient is more robust and resistant than the Pearson correlation, which one is commonly used. Spearman correlation measure the monotone dependence for continuous variables and it reflects the association between these variables (Freund and Wilson, 2003; Wilks, 2019). Only correlations with a confidence interval of 95 % (95 % CI) are considered. The statistics were calculated only for pixels with the highest Quality Assurance (QA) flags, which refers to QA = 3 for MxD04 products and QA = 0000 for MCD19A2 products.

The products ensembles were calculated with the spatial mean (median) of each product inside the 0.5 × 0.5 box, then with these values were calculated the mean (median) between the products. The value was calculated only when all products considered in that member were available, which is the MxD_DT, MxD_DB and MxD_MAIAC to MxD_3Ens, and MxD_DT, MxD_DB, MxD_MAIAC and MxD_3k to MxD_4Ens. It was considered only the pixels with best QA in the same satellite overpass.

The Dark Target algorithm allows small negative values of AOD. Even though this is physically unrealistic, they are considered to not introduce a bias. The negative values can be found in atmospheric clean conditions and arises from errors in assumptions of surface conditions, aerosol properties or calibration expectations (Levy et al., 2013; Remer et al., 2005; Sayer et al., 2014).

To analyze the spatial and temporal behavior of AOD retrieval across the algorithms, the swath data in the HDF files from MxD_DT, MxD_DB, MxD_DTDB and MxD_3k were filtered based on the highest quality flag. The data were then interpolated to a horizontal regular grid with resolution of 10 km (for DT, DB and DTDB) and 3 km (3 k), and the monthly

Table 5
Number of pixels inside the 0.5° x 0.5° box centered and collocated with AERONET AOD550 data from the site at Natal/RN with valid values and best quality control flags for each AOD product and its respectively mean AOD.

Product	Pix Count		Mean AOD Valid pixels (All QA)	Mean AOD Best QA
	Valid	Best QA		
MOD_DT	167	32	0.180	0.155
MOD_DB	90	7	0.248	0.126
MOD_DTDB	122	32	0.152	0.155
MOD_3k	1046	201	0.164	0.167
MOD_MAIAC	69,260	28,298	0.204	0.184
MOD_3Ens_MEAN	–	1446	–	0.087
MOD_3Ens_MEDIAN	–	1446	–	0.072
MOD_4Ens_MEAN	–	1495	–	0.081
MOD_4Ens_MEDIAN	–	1495	–	0.071
MYD_DT	478	85	0.115	0.130
MYD_DB	380	19	0.207	0.137
MYD_DTDB	258	85	0.135	0.130
MYD_3K	2373	1114	0.119	0.104
MYD_MAIAC	52,379	17,912	0.213	0.194
MYD_3Ens_MEAN	–	1977	–	0.124
MYD_3Ens_MEDIAN	–	1977	–	0.133
MYD_4Ens_MEAN	–	2217	–	0.110
MYD_4Ens_MEDIAN	–	2217	–	0.102
MERRA	–	875	–	0.114

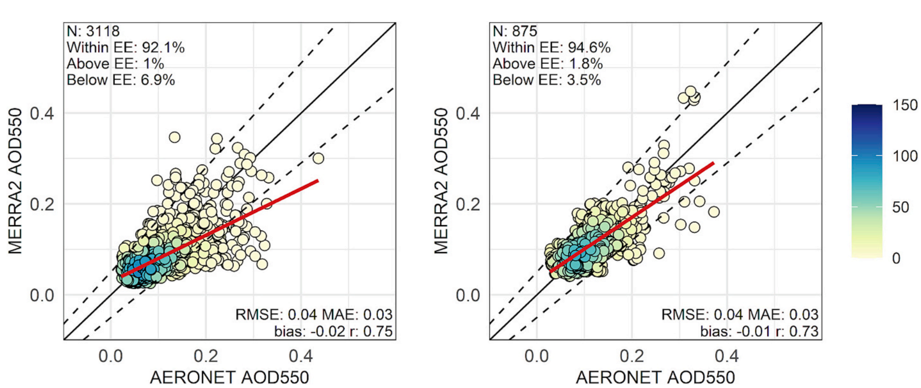

Fig. 4. Scatterplot of AOD550 from MERRA2 as a function of AERONET measurements for Petrolina/PE (left) and Natal/RN (right). The black solid line is the 1:1 line. The dashed lines are the expected error (EE) interval. N is the sample size, EE is the percentage of the samples within (=EE), under(<EE) or above (>EE) the expected error interval.

Table 6
Statistics of the comparison between AERONET AOD550 measurements and MODIS C6.1, from Terra (MOD) and Aqua (MYD), Dark Target 10 km (DT), Deep Blue (DB), DTDB, Dark Target 3 km (3 k), MAIAC AOD products, the ensemble products 3EnsMEAN, 3EnsMEDIAN, 4EnsMEAN, 4EnsMEDIAN, and MERRA2 over Natal/RN. EE is the percentage of the samples within (EE), under(<EE) or above (>EE) the expected error interval, sample size (N), RMSE, MAE, bias and Spearman correlation (r) with 95 % CI. Darker colour indicates the best result of each index.

Product	Statistics							
	N	%<EE	%EE	%>EE	RMSE	MAE	bias	r
MOD_DT	15	0	67	33	0.06	0.04	0.04	0.63
MOD_DB	1	-	-	-	-	-	-	-
MOD_DTDB	15	0	67	33	0.06	0.04	0.04	0.63
MOD_3K	42	5	50	45	0.10	0.07	0.05	-
MOD_MAIAC	107	1	59	40	0.10	0.07	0.07	0.59
MOD_3EnsMEAN	1	-	-	-	-	-	-	-
MOD_3EnsMEDIAN	1	-	-	-	-	-	-	-
MOD_4EnsMEAN	1	-	-	-	-	-	-	-
MOD_4EnsMEDIAN	1	-	-	-	-	-	-	-
MYD_DT	22	5	91	5	0.06	0.04	0.00	0.56
MYD_DB	6	-	-	-	-	-	-	-
MYD_DTDB	22	5	91	5	0.06	0.04	0.00	0.56
MYD_3K	53	17	79	4	0.06	0.05	-0.02	0.61
MYD_MAIAC	93	1	46	53	0.11	0.09	0.08	0.37
MYD_3EnsMEAN	5	-	-	-	-	-	-	-
MYD_3EnsMEDIAN	5	-	-	-	-	-	-	-
MYD_4EnsMEAN	5	-	-	-	-	-	-	-
MYD_4EnsMEDIAN	5	-	-	-	-	-	-	-
MERRA2	875	4	95	2	0.04	0.03	-0.01	0.73

mean AOD was calculated for each grid cell, alongside the sum of pixels contributing to each grid point. MxD_MAIAC data were similarly filtered for the highest quality flag, with monthly mean AOD and pixel counts calculated per grid cell. Subsequently, all products, including MERRA2, were clipped using the shapefiles for each biome and entire NEB region from IBGE (Instituto Brasileiro de Geografia Estatística) (reference year of 2019), and then spatially averaged to estimate the monthly mean AOD within each clipped area. The AOD monthly mean from MERRA2 was calculated using the values available at 12 UTC and 15 UTC, on its original spatial resolution. This database was prepared to serve as additional comparison. To calculate the correlation and mean differences matrices between products, the MxD_3k and MxD_MAIAC products were interpolated to match the 10 km grid of the other products. For the additional comparisons with MERRA2 data, all MODIS products were interpolated to align with the MERRAS2 grid.

3. Results and discussion

To evaluate the described AOD products over the NEB region, we present a collocated and regional analysis. The first one is a comparison between MODIS and AERONET AOD data, where the AERONET data is considered the “truth”. In the second analysis we compare the products for each NEB biome (Fig. 1). The biomes are assumed as homogenous groups in terms of surface characteristics. However, we recognize that these biomes are not fully preserved. In all of them, there are different land cover and land use categories as urbanization and conversion to agriculture and livestock. These analyses were performed considering only pixels with high-quality QA flag.

3.1. Validation comparing AERONET and MODIS AOD

3.1.1. Petrolina site in the state of Pernambuco

Petrolina city is located in the Caatinga biome, within the semi-arid region of the NEB. The counting of pixels inside a box of 0.5° x 0.5° centered at the AERONET site coordinates in Petrolina/PE and collocated with AERONET AOD data are shown in Table 3. For each product, the number of valid and best QA pixels from Terra is higher than from Aqua, except for the MAIAC algorithm. DB is the 10 km resolution product with the highest number of valid and best QA pixels. Both MxD_DTDB products have the highest percentage of best QA regarding valid pixels (99 %). These results were expected as the DTDB algorithm selects the high-quality pixels either from DT or DB. The MYD_DT shows the lowest one (43 %). When accounting for all products, the high-quality data set (Best QA) contains about 23 % less than all available valid pixels. A similar comparison was made by Gupta et al. (2018) on a global scale, who found 20 % fewer pixels for all QA when compared with the best QA.

The products MxD_MAIAC and the MxD_3k are of a higher spatial resolution of 1 km and 3 km, respectively. For this reason, they have more pixels than the 10 km products. However, the MAIAC product shows a much higher quantity of valid and best QA pixels, which is not only related to its higher resolution. For example, considering only the difference in resolution from 3 km (MxD_3k) to 1 km (MxD_MAIAC), a nine-fold increase would be expected. Instead, over sixty times more valid pixels and almost fifty times more best QA pixels were found. This shows that the quality control method of the MAIAC algorithm can select more pixels with good QA than the MxDL2 products. The AOD mean considering all QA varies between −0.01 (MYD_DT) to 0.153 (MYD_MAIAC), with similar values for Aqua and Terra when comparing the corresponding products. When considering only the best QA pixels the AOD means are smaller than those for all QA pixels, with values ranging between −0.022 and 0.124.

Comparing the AOD from the MODIS products with the AOD provided by AERONET data, shown in the Fig. 3, and summarized in Table 4, reveals that satellite products tend to underestimate the AOD: the number of AOD values below the EE range is much higher than those above. This is also reflected by the bias, which is all negative. Between the MODIS products, the MOD_DB and MYD_DB products show the best results, with 95 % and 86 % of the data within the EE, respectively. This is also corroborated by RMSE of 0.04 and 0.05, MAE of 0.03, biases of −0.01 and − 0.03, as well as correlation coefficients of 0.74 and 0.48. From Terra, these are the overall best results. Regarding Aqua products, even though MYD_DB yields the best results, the correlation of MYD_3k is similar. However, only 28 % of the data lies within the EE range and show higher RMSE, MAE and bias. Both MxD_DT products yielded the highest percentage of underestimates (<EE). As expected, the combined products (MxD_DTDB) lie between the DT and DB results, with values closer to DTs. The Terra product MOD_DB (95 % within EE range) performs better than the Aqua product MYD_DB (86 % within EE range). However, for the DT and DTDB products, data from Aqua shows slightly better results than from Terra. The MxD_DT products and MxD_3k, also based on the DT algorithm, have the highest RMSE and MAE. These results indicate that the pure Dark Target product is not able to represent well the AOD for this region. MxD_MAIAC shows good results as well, and it is the only product overestimating the AOD, with a positive bias. However, the MAIAC product has the advantage of its higher resolution, offering a larger sample. Only the MxD_DB, MxD_MAIAC products, as well as the ensembles provide more than 66 % of the AOD values within EE. The average errors of the products for each satellite presents similar values for Terra and Aqua, with a mean RMSE of 0.09, a mean MAE of 0.08 and a mean bias of −0.06. For both satellite products, there is a tendency to underestimate the AOD values when compared to the AOD from AERONET, except MAIAC. The ensembles products show results, specially the MxD_3Ens. The MOD_3EnsMEAN and MOD_3EnsMEDIAN present similar results, except to EE, where the median ensemble shows 94 % of the data within EE, while the mean ensemble shows 71 %. Due the restriction that all products considered in each ensemble must have at least 1 pixel available, the MxD_4Ens show a smaller N than MxD_3Ens, because the 4Ens would need the same AOD products as the 3Ens add the MXD_3K.

The AOD reanalysis from MERRA2 shows a good agreement with AERONET AOD, indicating that this database can be used for AOD studies over the region, with the advantage of providing a more regular space-time characterization (Fig. 4 - left). However, the spatial

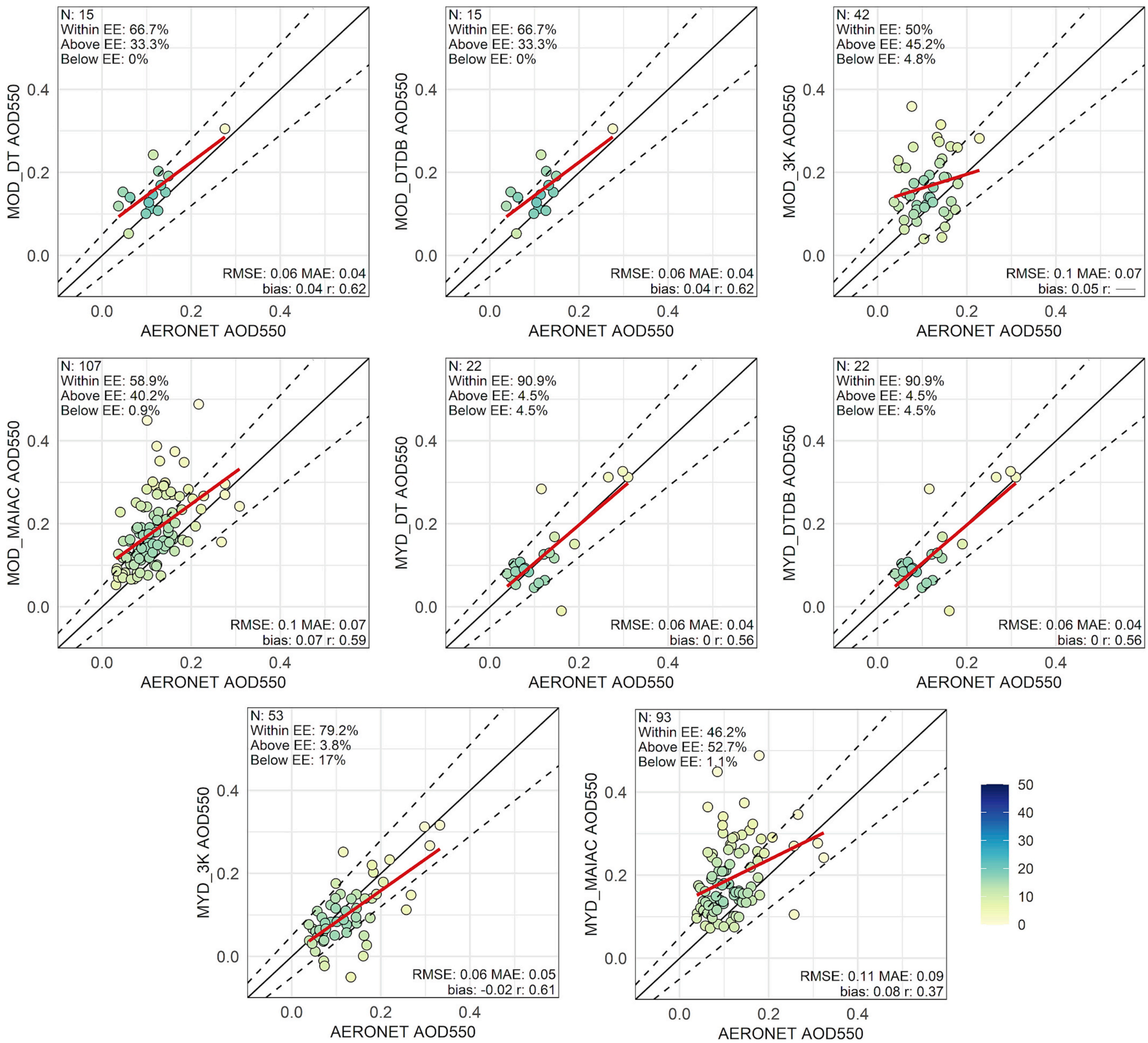

Fig. 5. Scatterplot of AOD550 from Aqua and Terra MODIS C6.1 Dark Target 10 km (DT), DTDB, Dark Target 3 km (3 k) and MAIAC as a function of AERONET AOD measurements over Natal/RN. The black solid line is the 1:1 line. The dashed lines are the expected error (EE) interval. N is the sample size, EE is the percentage of the samples within (=EE), under(<EE) or above (>EE) the expected error interval. (For interpretation of the references to colour in this figure legend, the reader is referred to the web version of this article.)

resolution of 0.5° x 0.625° (~50 km close to the Equator) of MERRA2 is much coarser than the MODIS AOD products (1 to 10 km). It is also worth mentioning that MERRA2's good performance is highly influenced by its assimilation of some of these observations discussed here, namely the radiances of DT products (Randles et al., 2017). The superior performance of DB products, when compared with DT, indicates that a regionally customized assimilation of MODIS AOD products by MERRA2, according to their errors, can improve its AOD analysis.

3.1.2. *Natal site in the state of Rio Grande do Norte*

Natal is on the eastern coast of the NEB, within the Atlantic Forest biome. The numbers of valid and best QA pixels and AOD mean at the AERONET site in Natal/RN, within the 0.5° x 0.5° and temporally collocated with the AERONET data, are shown in Table 5. There are very few valid and best QA pixels for the 10 km products. The best QA pixel of MAIAC represent 41 % (MOD) and 34 % (MYD) of all valid pixels. The MYD_3K present the highest proportion, with 47 % of all pixels benign best QA, and the MxD_DB with the lowest percentage. On the average, the MYD products present a higher percentage of best QA in relation of valid pixels. Due to the site location at the Atlantic coast, situated 2 km from the shore, it is marked by the transition between land and ocean, where the MODIS AOD products historically miss or produce highly biased AOD (Wang et al., 2021). In addition, DB algorithm only retrieval AOD over land. The proportion of the number of valid and best QA of MxD_MAIAC and the 10 km products presents similar results of Petrolina site. The number of MxD_MAIAC pixels is more than a hundred times of 10 km products, showing that the number of pixels is not only due the higher resolution. The total amount of valid pixels and best QA are higher in Aqua's product, except of MAIAC. This behavior is the opposite of what occurred to Petrolina. The AOD mean when considering all valid

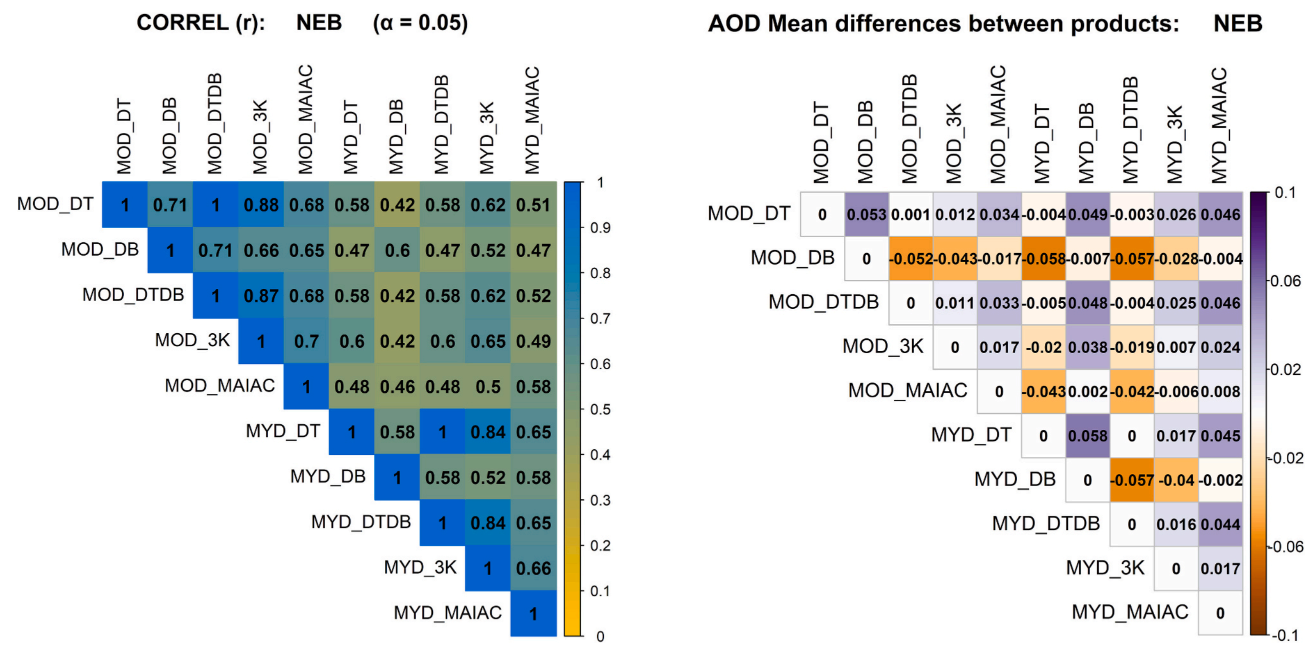

Fig. 6. Correlation matrix of AOD550 with significance level α = 0.05 (left side) and AOD550 mean differences (column minus row; right side) between MODIS AOD550 products to the NEB region between 2015 and 2018.

pixels ranges between 0.115 (MYD_DT) and 0.248 (MOD_DB). If only the best QA pixels are considered, the AOD mean ranges between 0.1 (MYD_3K) and 0.19 (MYD_MAIAC). Similar AOD values were found by dos Oliveira et al. (2021) who used AERONET AOD data from the Natal/RN site, with values ranging between 0.10 and 0.15. The MOD_3Ens and MOD_4Ens shows a mean AOD smaller than the MOD products. This value is not representative due to the restriction of all products must be available to calculate the mean and median, in this case there is only one value calculated.

The MAIAC algorithm was capable of retrieve a large number of AOD pixels at the coastal region of Natal. The comparison with AERONET data with both MOD_MAIAC and MYD_MAIAC, shown in Table 6 and Fig. 5, display weaker performance compared to their corresponding Dark Target products, with higher RMSE (0.10–0.11) and lower correlations (0.59 for Terra, 0.37 for Aqua)… and a positive bias of 0.07 (MOD) and 0.08 (MYD), which are a little higher to those of Petrolina. This suggests that MAIAC may not be as reliable for AOD retrieval in this specific region. MYD_DT and MOD_DT are fairly comparable in terms of RMSE (both 0.06), MAE (0.04), and bias (close to 0). However, MYD_DT performs slightly better in terms of the percentage within the expected error range (91 % vs. 67 %) and correlation ($r = 0.56$ vs. 0.63 for Terra). To the site in Natal, the products show a tendency of overestimate (positive bias) the AOD from AERONET, except the MYD_3K. The Spearman correlation of MOD_3K is not shown due its p value smaller than the confidence level of 0.05. The ensembles and MxD_DB are not shown due its small sample (N). As in Petrolina, MERRA2has the highest number of samples ($N = 875$) and shows very strong performance across most metrics. It has the highest percentage of data within the expected error range (95 %), the lowest RMSE (0.04), and a solid Spearman correlation ($r = 0.73$), which makes it reliable to use on the region.

Sayer et al. (2014) analyzed DB, DT, and DTDB from MODIS collection 6 for Central- and South America and found that all of the products showed correlations with AERONET close to 0.9, and a RMSE of 0.14, a mean bias of −0.022, −0.033 and − 0.032, respectively. The amount of data within the EE was 73 %, 54 %, and 56 %, respectively. The authors also show that the DB presents a better performance to the Petrolina site. Gupta et al. (2018) showed that the DT products from Terra, for both 10 km and 3 km resolution, presented a mean bias 0.03 higher than Aqua, and concluded that the 3 km product is less accurate than the 10 km one. This result was previously found by Remer et al. (2013). Lyapustin et al. (2018) validated MAIAC data and found a correlation with the AERONET site at Petrolina of ~0.4, RMSE of ~0.06, and a bias of ~0.2.

3.2. Regional analysis

The daily AOD550 values of the analyzed products were monthly and spatially averaged for the entire NEB region and individually for each biome. First, we discuss the results for the entire NEB region and subsequently those for each specific biome.

During the four analyzed years, relatively low mean values of AOD were obtained considering all of the NEB region. The mean of all AOD data from Terra is 0.095, while Aqua's AOD mean is 0.091. Analyzing the products individually, the AOD mean of the four years ranges from 0.03 ± 0.08 (MYD_DT) to 0.09 ± 0.06 (MYD_MAIAC). The distinct AOD products from Terra (DT, DB, etc.) present a higher correlation among themselves when compared with the correlation among the same products from Aqua. This can be seen in Fig. 6, as well, as a correlation matrix for the AOD mean from distinct products all over the NEB region. The average correlation coefficient between all Terra products is 0.75 compared to Aqua products with a correlation coefficient of 0.69. The MAIAC AOD shows a better correlation with 3 k products than the other products. This can be due to the higher spatial resolution that both have, retrieving AOD with higher details than the 10 km resolution. The correlation between DT and DB is better for Terra (0.71) than for Aqua (0.58) products. Comparing the correlation of the satellites (MOD x MYD) to each product, the 3 k product shows the highest correlation, followed by DB correlation.

The merged DT and DB product (DTDB) has a correlation of 1 with the DT product, for both satellites. This indicates the prevalence of AOD values from the DT algorithm, instead of those from DB in the merged DTDB product. This result was expected due to the DTDB algorithm choice map (Sayer et al., 2014), which indicates that in almost all NEB area, the algorithm uses DT data every month. There is a small region in Caatinga area where the algorithm merges DT and DB some months. This case will be discussed in more detail later. The DTDB choice map partially agrees with the NDVI values shown by da Silva et al. (2023) in the NEB region, where the NDVI ranging from −0.69 to 0.85, where

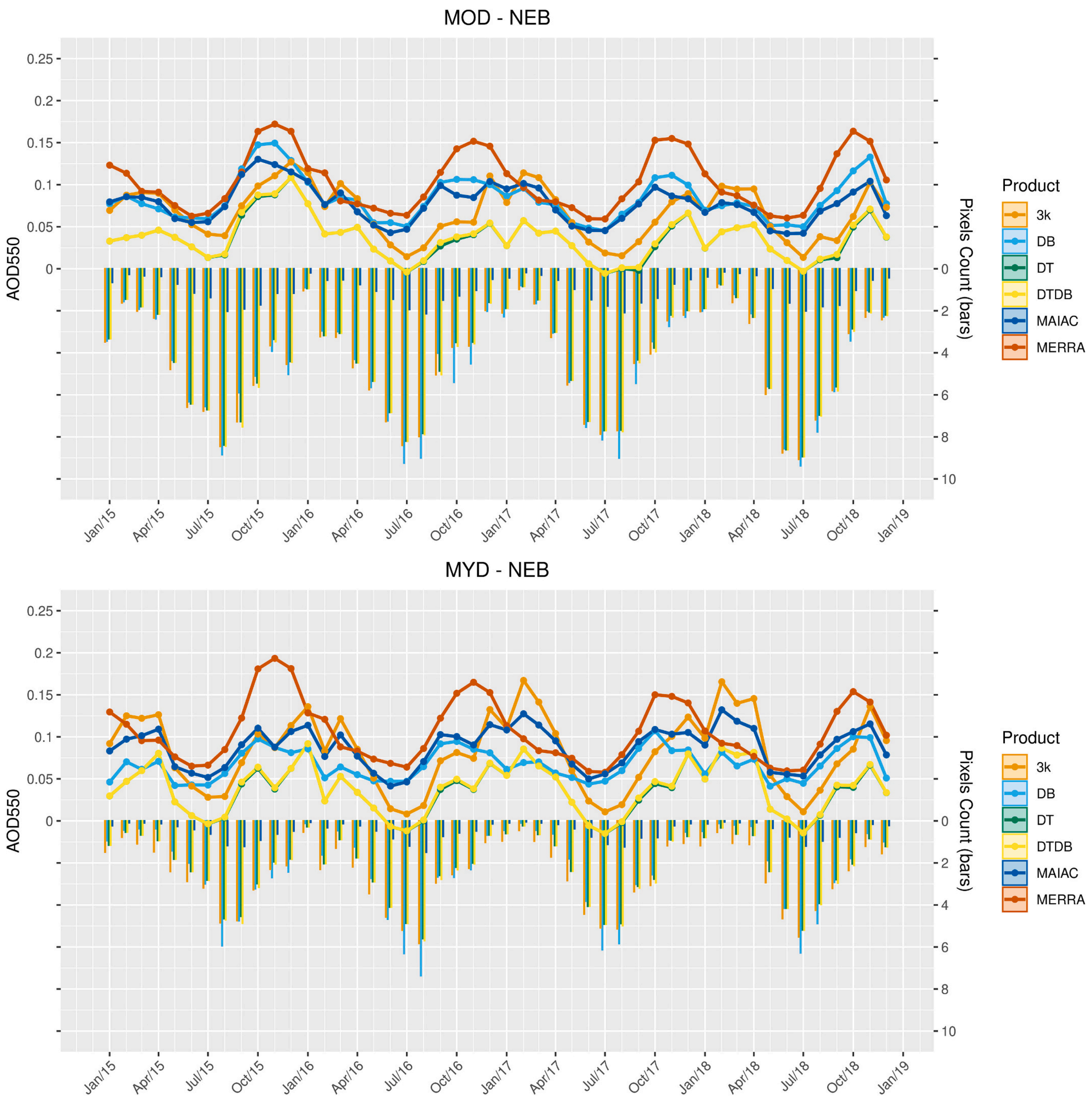

Fig. 7. Seasonal pattern of AOD550 with monthly mean (colored lines) and number of pixels (bars) for the NEB region from 2015 to 2018 for Terra (MOD) and Aqua (MYD) satellites products. There are scale factors in the pixels count scale of 10^4 (DT, DB, DTDB), 10^5 (3 k), and 10^7 (MAIAC). (For interpretation of the references to colour in this figure legend, the reader is referred to the web version of this article.)

−0.69 to −0.01 are identified as water bodies. Areas with little or sparse vegetation range from 0.00 to 0.40, such as the Caatinga biome. Regions with dense vegetation during most of the year show NDVI values from 0.43 to 0.85.

To include the MERRA2 AOD analysis in the correlation matrix, all data was interpolated to MERRA2's grid (not shown). MERRA2 has a good correlation with DB and DT products (> 0.60). MERRA2's lowest correlation is with MYD_MAIAC (0.47). The monthly AOD from MERRA2 at 12 UTC and 15 UTC are very similar, with a mean difference of −0.002 (MERRA2_12UTC minus MERRA2_15UTC). Analyzing this difference in each biomes, the values are also very small, with 0.005 in the Amazon, −0.007 in the Atlantic Forest, 0.003 in the Caatinga, and 0.003 in the Cerrado. Due this reason, on the figures to each biome, the MERRA2 values to MOD and MYD seems very similar.

Analyzing the Fig. 6 (right), where we show mean difference of the product in the column minus the product in the row, the mean difference of AOD values between the products in we can see that the highest differences occur between DB and DT products, with DB in general being higher than DT (differences around 0.05). This result is consistent with Sayer et al. (2014) who found values of AOD DT minus AOD DB between 0.05 and 0.1 in the Caatinga and Cerrado biomes of Brazil. The mean difference between DT and DTDB is close to zero. The MxD_MAIAC and MxD_DB products show only small differences.

Regarding the interannual variability for the analyzed period, all

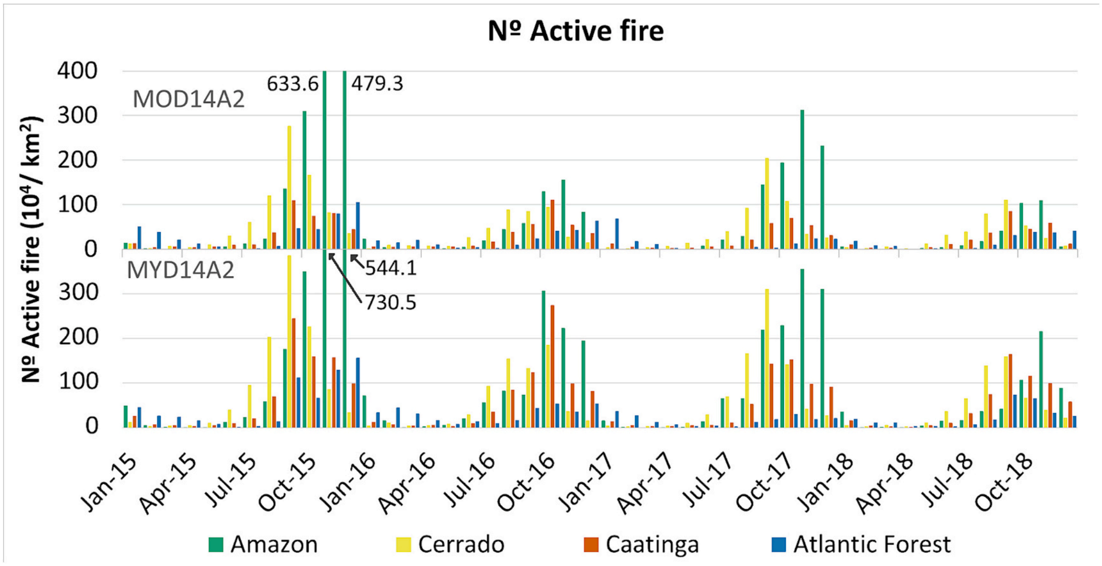

Fig. 8. Monthly density of active fires (fire foci normalized by the area of each biome) in NEB region from 2015 to 2018, using the MODIS products MOD14A2 and MYD14A2.

AOD products show a similar pattern, with the primary difference being the timing of maximum values (Fig. 7). All products converge on a maximum in Nov/2018. However, for the remaining period, patterns diverge MxD_DB products reach peak AOD values in Oct-Nov, while MxD_DT, MxD_DTDB and MxD_3k products exhibit peaks between December and April. The MxD_MAIAC show an annual trend like MxD_DB, yet they follow peaks observed in both DB and DT products. The MxD_DT, MxD_DTDB, and MxD_3K present minimum values in Jun-Jul-Aug, whereas MxD_DB, MxD_MAIAC, and MERRA2 reach the minimum values in May-Jun-Jul. The MERRA2 shows elevated AOD values in Oct-Nov. The number of pixels with high QA of AOD product also reveals clear seasonality, with the highest counts in Jul-Aug and the lowest in Jan-Feb. These pixels distribution aligns with the seasonality of precipitation in NEB's semi-arid region (Oliveira et al., 2017), marked by a rainy season during Dec-Jan-Feb and a dry period during Jun-Jul-Aug. This will be further discussed in more detail when we analyze each biome.

In the NEB region, the agriculture and livestock are the primary drivers of forest fires. Among the Brazil's five regions, NEB ranks second in fire foci occurrence, contributing 27.1 % of the national total. (Caúla et al., 2015). During the study period, fire activity (Fig. 8) shows a marked increase in Sep-Oct-Nov-Dec across all biomes, with a decline in January. In the Amazon, the fire activities are concentrated in Oct-Nov-Dec, with significant peaks in 2015 and 2017. November 2015 marks the highest fire foci counts across the datasets, suggesting a particularly severe fire season that year. In the Caatinga, the fire activity also peaks in Sep-Oct-Nov, with high values in 2015 and 2017. The Cerrado area exhibits high fire activity primarily in Aug-Sep-Oct, with values peaking in 2015, 2017, and moderately in 2016, consistently showing some of the highest fire occurrences compared to the other biomes. The Fire activity in the Atlantic Forest region is comparatively lower, displaying more consistent, less variable patterns, although with prominent peaks in September 2015 and 2017.

A comparison of AOD patterns and fire activity in NEB shows that peal AOD values in MxD_DB products align with months of heightened fire activities in Caatinga. Meanwhile, peaks in the AOD products based on the Dark Target algorithm in November correspond with intense fire periods in Amazon. Another possible reason for this time discrepancy between AOD maxima may be the number of high-quality pixels available per product. This is illustrated in the Fig. 9 and Fig. 10, which presents the monthly mean AOD of MxD_DT, MxD_DB, MxD_3k, MxD_MAIAC and MERRA2 in October and December of 2015. This year were selected only as an example, however there is similar results across the remain years. The Deep Blue products demonstrate a limited AOD representation over the Amazon and surroundings areas compared to Dark Target and MAIAC products. However, DB offers great AOD coverage over Caatinga relative to DT products. In contrast, Dark Target products show fewer AOD retrievals in Caatinga than Cerrado and Amazon, proportionate to biome area. These discrepancies affect the mean AOD for the entire NEB region, contributing to timing differences among the product maxima. This effect is also evident in October, when MxD_DTDB values are slightly higher than those of MxD_DT due to the increased number of AOD retrievals selected from DB in Caatinga region, aligning more closely with DB's mean AOD. In December, high AOD values across eastern NEB, particularly in Amazon and Cerrado, skew the mean AOD to reflect this area more prominently.

3.3. *The Amazon biome in Northeast Brazil*

In the Amazon biome of the NEB, the minimum number of pixels for all satellite products is observed in Jan-Feb-Mar (Fig. 11). Due to its small area, there are periods with few high-quality pixels available, with an extreme case in February 2018, when the MYD_DB product presents 0 pixels. The maximum number of pixels can be found for the month of July, for both high-resolution (MxD_MAIAC) and coarser-resolution products. This seasonality in the number of pixels is consistent with the precipitation cycle pattern shown by Correia Filho et al. (2019), Oliveira et al. (2017), and Paredes-Trejo et al. (2017), with the lowest number of pixels occurring during the months of the rainy season (January–April), and highest number observed during the dry season (July and September). The mean seasonal variability of each AOD product in the portion of the NEB region that corresponds to the Amazon biome is presented in Fig. 11. In general, MOD and MYD present a consistent seasonality, with minimum values occurring during JJA and AOD increasing from September and peaking in November/December. The AOD MERRA2 peak in November presents a sharper decrease when compared to the AOD of the satellite products. Also, it presents a minimum period, from March to July, larger than that of the satellite products. For the latter, the lowest AOD occurs during Jun-Jul-Aug, with the minimum values varying from 0.04 (MOD_DTDB) to 0.05 (MYD_DTDB). The highest values occur in Nov-Dec-Jan, ranging from 0.38 (MYD_3k) to 0.39 (MOD_3K). The 3 K product presents the highest

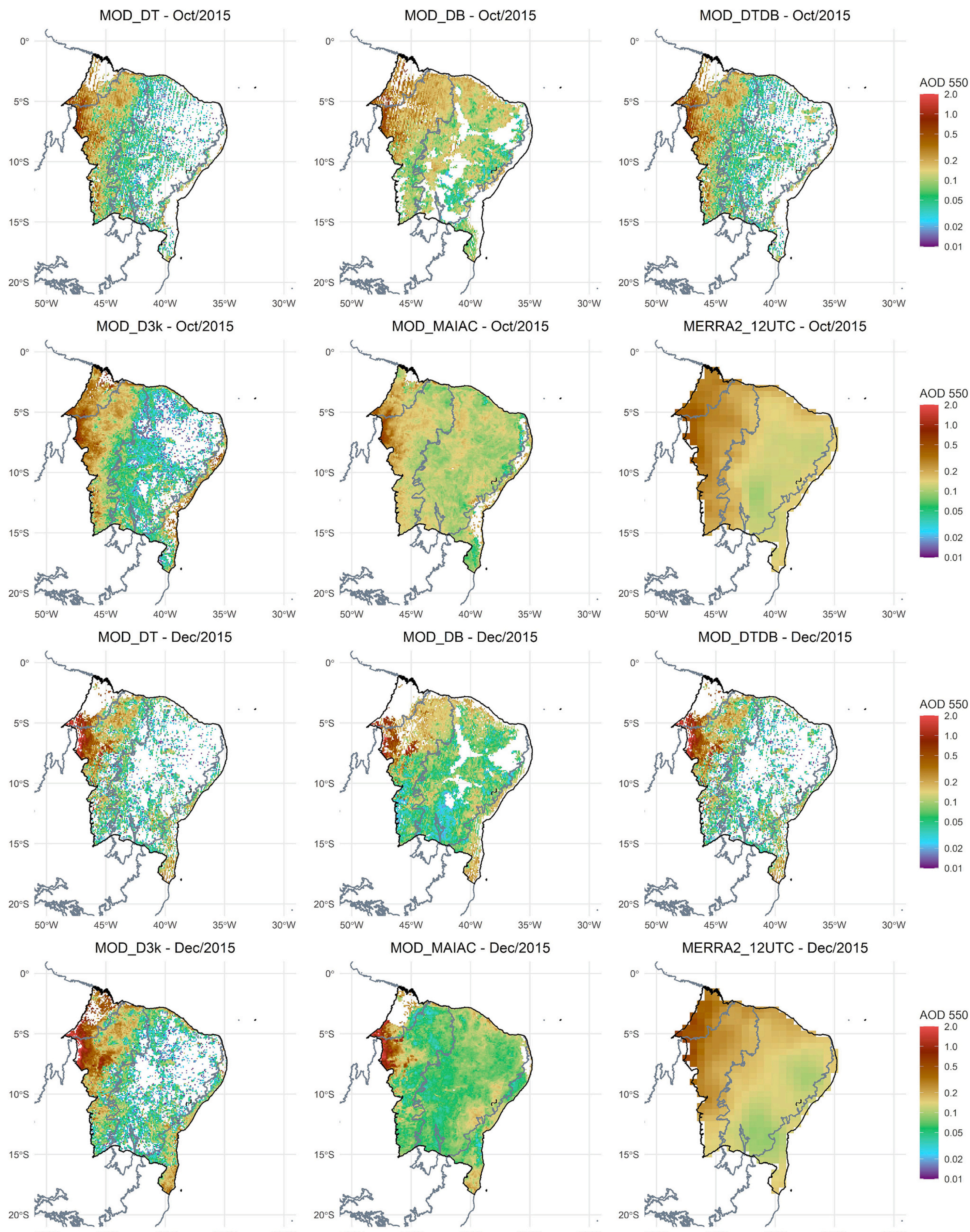

Fig. 9. Monthly mean AOD at 550 nm of MODIS/Terra products and MERRA2 in NEB region for October and December of 2015. Gray lines indicate biomes boundaries and black line delineates the NEB area.

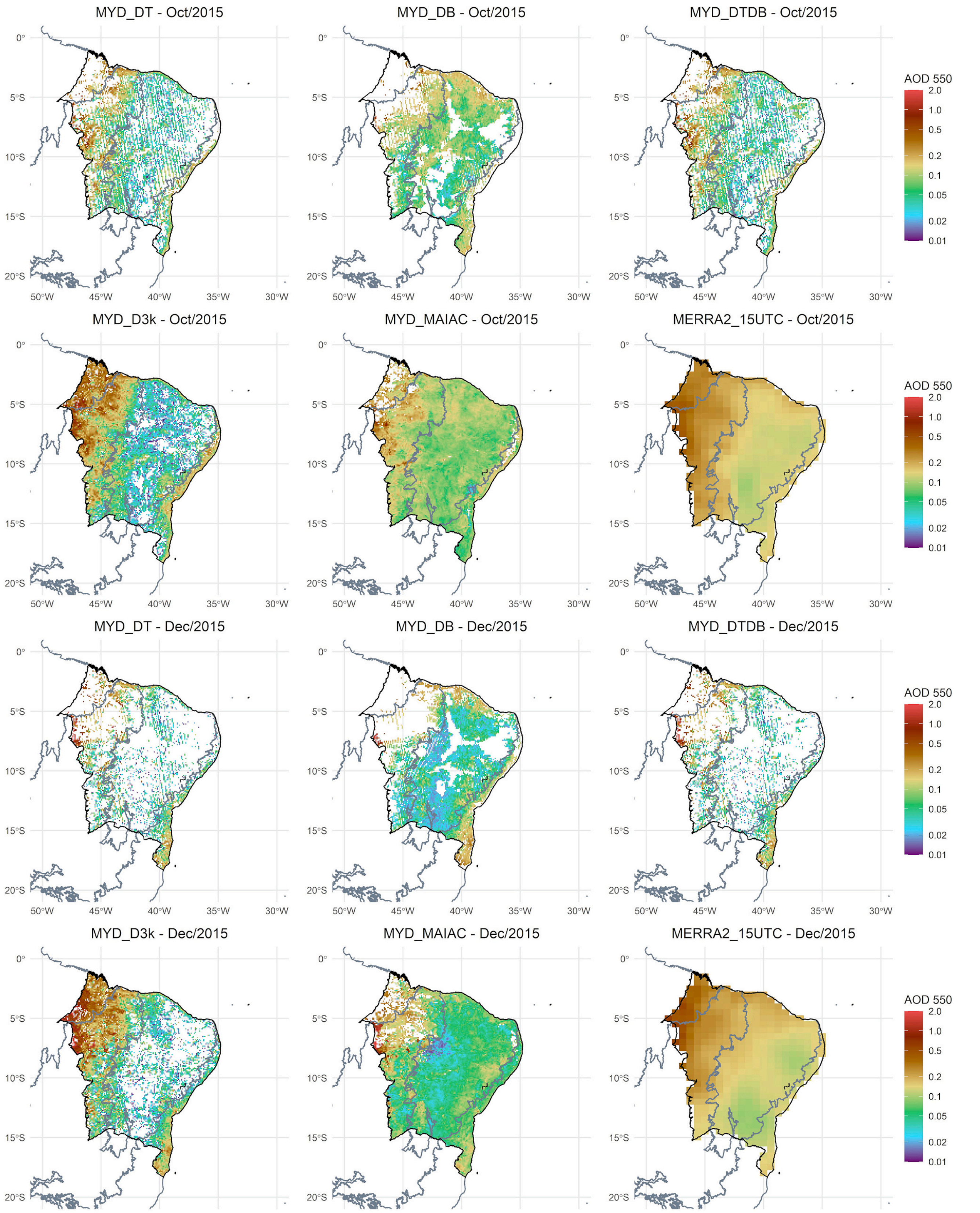

Fig. 10. Monthly mean AOD at 550 nm of MODIS/Aqua products and MERRA2 in NEB region for October and December of 2015. Gray lines indicate biomes boundaries and black line delineates the NEB area. (For interpretation of the references to colour in this figure legend, the reader is referred to the web version of this article.)

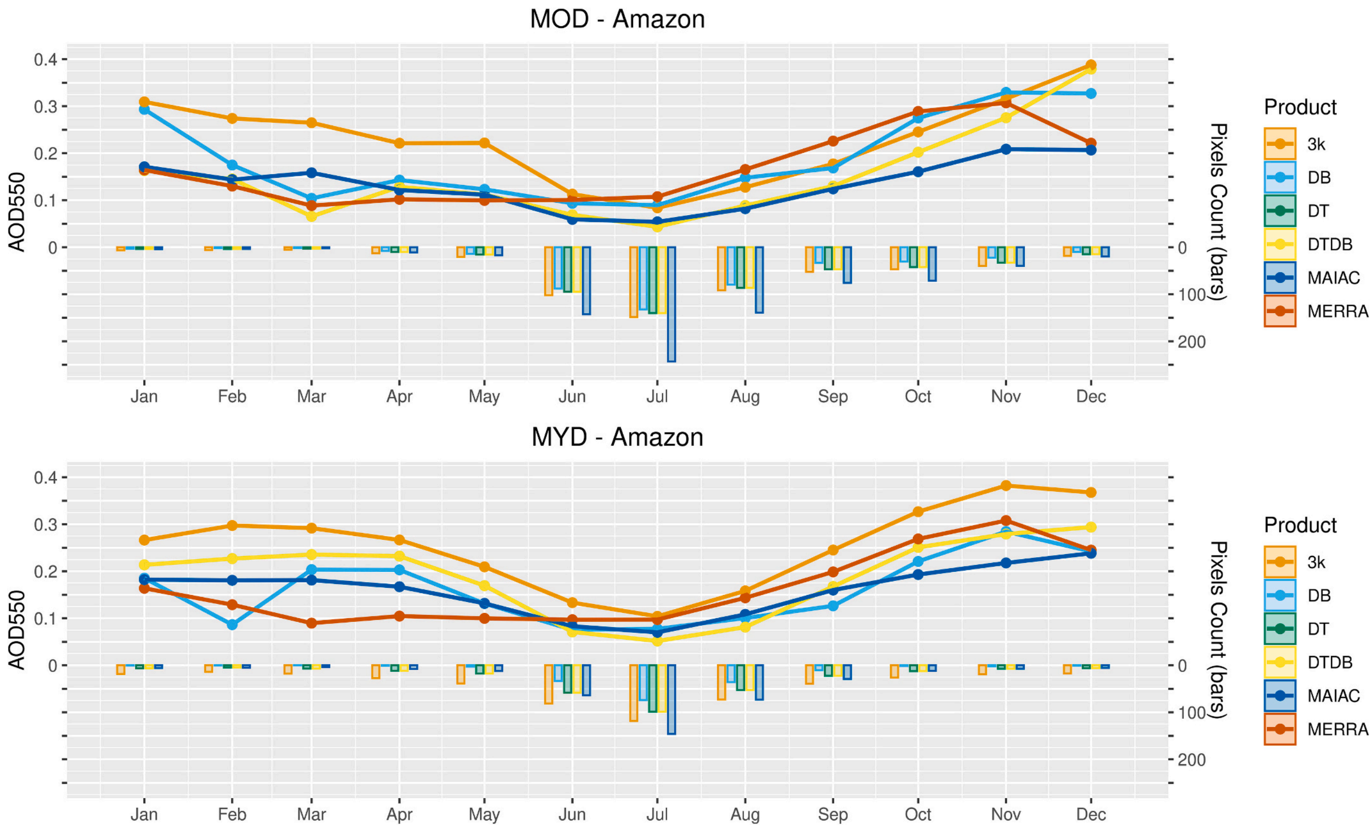

Fig. 11. Seasonal pattern of AOD550 with monthly mean (colored lines), and number of pixels (bars) in the NEB biome domain of Amazon from 2015 to 2018 for Terra (MOD) and Aqua (MYD) satellites products. There are scale factors in the pixels count scale of 10^2 (DT, DB, DTDB), 10^3 (3 k), and 10^4 (MAIAC). (For interpretation of the references to colour in this figure legend, the reader is referred to the web version of this article.)

values during almost all months. MERRA2 shows values of AOD smaller than almost all MODIS products between January until May, except in March when MOD_DT and MOD_DTDB are smaller, and in February when MYD_DB is smaller. From July until October, the MERRA2 AOD is the highest among the Terra products, and between the MYD_3K and the 10 km products. This region is affected by the biomass burning season of the northeast portion of Amazonia, which occurs later than the well-known Southern Amazon biomass burning season (Rosário et al., 2013). The number of fires in this part of the NEB starts to increase in August, and reach their peak in Oct-Nov-Dec (Fig. 8).

3.4. The Atlantic Forest in Northeastern Brazil

The NEB portions correspond to the Atlantic Forest biome extending along the coast, where nine out of 10 state capitals of the NEB are located. Hence, it is the most populated biome in the region. In general, the AOD is lower than for the Amazon biome in all products. There is a weak seasonal pattern, with minimum AOD values in April and May (Fig. 12). All MODIS and MERRA2 products show a very similar pattern and values, except for the MOD_3k which presents the highest AOD for all months. The MYD_DT and MYD_DTDB products have the lowest AOD values during all months. The products from Aqua have a better agreement among themselves than Terra's products. The monthly AOD among Terra's products range from 0.04 (MOD_DTDB) to 0.17 (MOD_3k), with a total average of 0.09. For Aqua, the values vary from 0.34 (MYD_DTDB) to 0.12 (MYD_3k), with an average of 0.08. Using data from an AERONET sun-photometer temporarily installed in Natal/RN (in the Atlantic Forest region), dos Oliveira et al. (2021) calculated a monthly average of AOD_{500nm} between 0.1 and 0.15 from Aug/2017 to Mar/2018. In their analysis the aerosol columnar load is composed mainly of marine aerosols, dust, and local and remote biomass burning. The number of high-quality pixels is at a minimum in February for both satellites' products, except for the MYD_DB for which the minimum occurs in April. All Aqua products show about 10 % more pixels than those of Terra. Contrary to the Amazon biome, the seasonal pattern of the number of pixels in the Atlantic Forest biome did not follow the seasonal climatology of precipitation in the region. In the northern part of the Atlantic Forest biome, the maximum monthly precipitation occurs typically in May and June, while for the southern part of the coast, the largest amount of precipitation is observed during November and December (Correia Filho et al., 2019; Oliveira et al., 2017; Paredes-Trejo et al., 2017).

3.5. The Cerrado biome in Northeast Brazil

In the Cerrado region of the NEB, for Terra's satellite products, the extreme monthly AOD varies between 0.004 (MOD_DT) in July, and 0.157 (MOD_DB) in November (Fig. 13). All Terra products present a similar seasonal pattern, with minimum values in July, except for the MAIAC product with its minimum in June, and its maximum in November. MOD_DB and MOD_MAIAC show close AOD values over the year, but from September to December MOD_DB AOD increases faster than the MOD_MAIAC product. MYD_DB and MYD_MAIAC AOD are very close between June and November, and differ on January until April, when MYD_MAIAC presents a higher AOD than MYD_DB. For the same period MOD_DB AOD is higher than that of MOD_MAIAC. The minimum AOD from Aqua's products occurs in June/July, with the lowest AOD of −0.014 obtained for MYD_DT. The maximum AOD is 0.187 registered by MYD_3k in December. In NEB's Cerrado the number of fire foci starts to increase in August, reaching its maximum in September (Fig. 8). MERRA2 shows values higher than the satellite products (MOD and MYD) for the second half of the year, with a maximum in October and

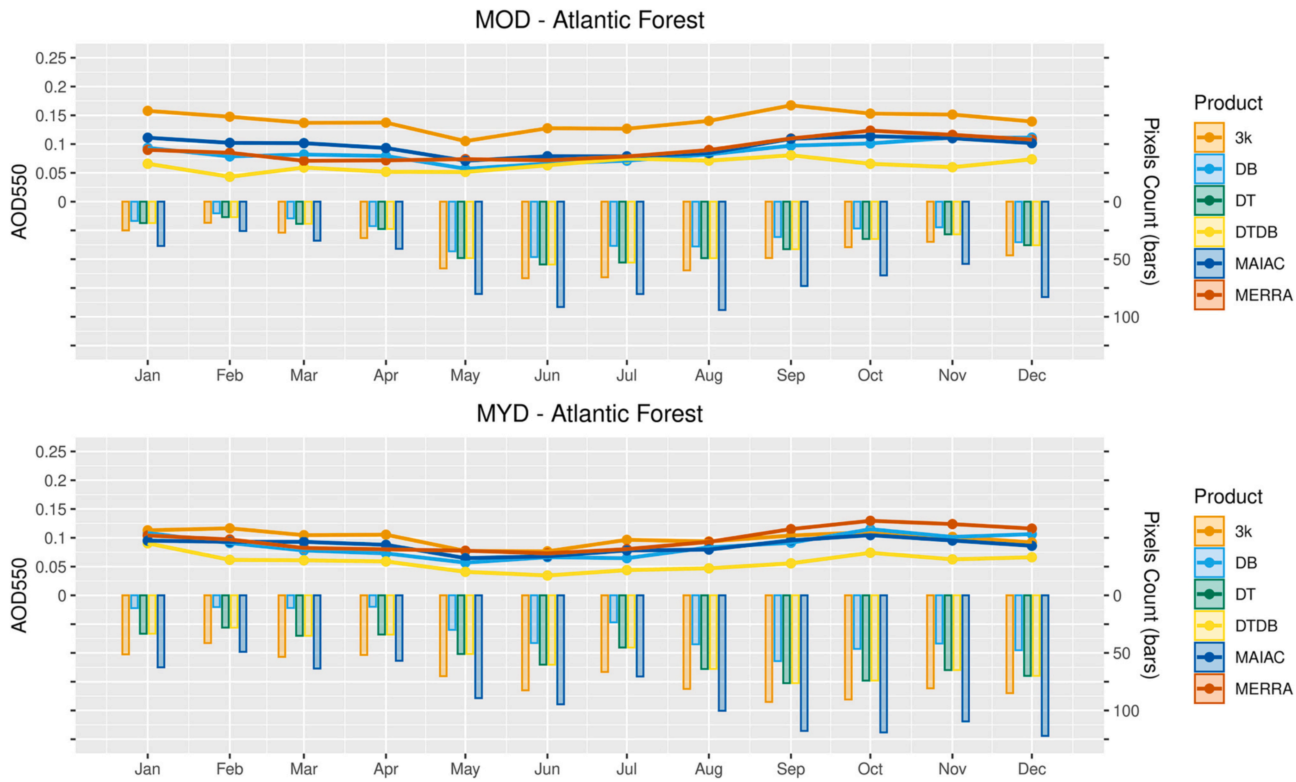

Fig. 12. Seasonal pattern of AOD550 with monthly mean (colored lines), and number of pixels (bars) in the NEB biome domain of Atlantic Forest from 2015 to 2018 for Terra (MOD) and Aqua (MYD) satellites products. There are scale factors in the pixels count scale of 10^2 (DT, DB, DTDB), 10^3 (3 k), and 10^4 (MAIAC). (For interpretation of the references to colour in this figure legend, the reader is referred to the web version of this article.)

November. However, in the final trimester of the year, the predominant wind direction in the region is from E/SE, coinciding with a higher number of fire foci in the Caatinga and Atlantic Forest biomes, which are situated east of the Cerrado biome. Therefore, an important fraction of AOD measured by the MODIS products in this period can be due to the transportation of plumes emitted in the Caatinga and the Atlantic Forest. The MOD products show in total 42 % more high-quality pixels than those of MYD. However, all of them provide a similar pattern during the year, with a maximum in austral winter and a minimum in summer, which agrees with the rainfall seasonality of the Cerrado in the NEB region: a rainy period in Jan-Feb-Mar and a drier period in Jun-Jul-Aug (Correia Filho et al., 2019; Oliveira et al., 2017; Paredes-Trejo et al., 2017).

3.6. The Caatinga biome in Northeast Brazil

Caatinga is a unique biome and the most extensive of the NEB, covering almost 1/3 of its area. Comparing MODIS AOD products for this biome (Fig. 14), we can see that on average it presents the lowest AOD mean compared to all other biomes. The AOD mean for Terra products is 0.037, with a seasonality ranging between −0.017 in July (for the DT algorithm) and 0.093 in October (for the DB algorithm). For Aqua, the obtained AOD mean is 0.04, with a seasonality among the products ranging from −0.025 (for the DT in July) to 0.095 (for the MAIAC in March). Generally, the products based on the DT algorithm (MxD_DT and MxD_3k) and the MxD_DTDB present similar patterns with an AOD increase in Feb-Mar-Apr and a decrease in July, reaching negative values. MOD_DB and MOD_MAIAC AOD's have very similar values and patterns, with a difference in November when MOD_DB is higher than MOD_MAIAC. MYD_MAIAC shows higher AOD values than MYD_DB during all months, except for October when both products estimate an AOD of 0.09. The seasonal pattern of the MERRA2 AOD is similar to those of MxD_DB and MxD_MAIAC and shows a higher AOD in all months compared to the MODIS products, except in March and April, when MAIAC AOD increases and is higher than MERRA2 AOD. The Caatinga is the only biome where the DTDB shows perceptible differences compared to DT. This can be related to the low NDVI surface values that characterize the region. In this area, the DTDB choice map merges the DT and DB during some months. If the pixel shows a NDVI between 0.2 and 0.3, the DTDB algorithm uses the AOD retrieved with the higher QA from DB or DT, or the mean of these two if both return QA = 3. September to December is the period with a higher quantity of fire foci in the region (Fig. 8). This can explain the AOD s behavior during this period. The elevation of AOD during Feb-Mar-Apr in the NEB region has been related to the long-range transport of aerosols from Africa, due to biomass burning and Sahara dust (Formenti et al., 2008; dos Oliveira et al., 2021; Tsamalis et al., 2013; Weinzierl et al., 2011). Regarding pixel statistics, the lowest number of pixels occurs in the austral summer for all products, while the highest counts can be found in Jul-Aug-Sep. The largest number of pixels matches with the period with low precipitation, while the months with a lower number of pixels are found in the period with more precipitation (Correia Filho et al., 2019; Oliveira et al., 2017; Paredes-Trejo et al., 2017). As in the Amazon and Cerrado, the total number of pixels accounted for in the MOD products is higher than for the MYD products, with a difference of 28 %.

4. Conclusions

In this paper we analyze and discuss the aerosol columnar load over the Northeast of Brazil (NEB), estimated as AOD by different remote sensing platforms and as calculated by MERRA2. The NEB is the most diverse region in Brazil when it comes to biomes (Atlantic Forest, Amazon, Cerrado, and Caatinga) and comprises an area about three times the size of France. Consequently, the NEB region presents a vast variety of aerosol sources and surface features, which may be considered a critical aspect for AOD retrieval from satellite observation, which can

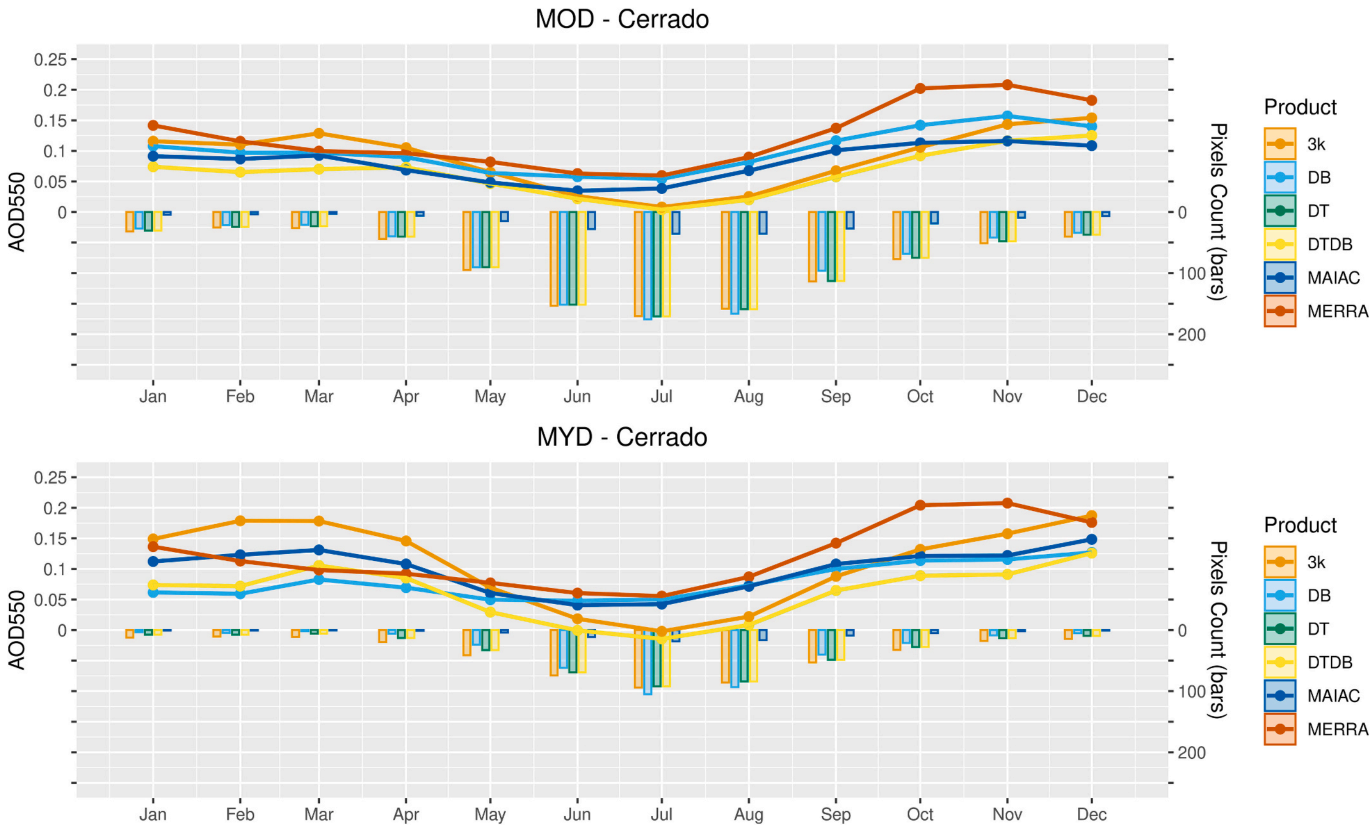

Fig. 13. Seasonal pattern of AOD550 with monthly mean (black dots), and number of pixels (bars) in the NEB biome domain of Cerrado from 2015 to 2018 for Terra (MOD) and Aqua (MYD) satellite products. There are scale factors in the pixels count scale of 10^3 (DT, DB, DTDB), 10^4 (3 k), and 10^6 (MAIAC). (For interpretation of the references to colour in this figure legend, the reader is referred to the web version of this article.)

be extremely complex. The analyzed remote sensing platforms are the AERONET sun-photometer and the MODIS instruments aboard both Terra and Aqua satellites, providing MODIS AOD daily products, currently producing collection numbered 6.1.

The MODIS-based AOD products comprise several approaches based on different algorithms, aiming to reduce the uncertainties, improve or adjust their accuracy and application. The traditional DT algorithm at 10 and 3 km resolutions explores low albedo surface (DT) to estimate AOD at regional and urban scales, respectively. The DB algorithm was developed targeting the improvement of AOD inversion over high albedo surface, such as the NEB semi-arid region. Finally, the more recent MAIAC product at high resolution (1 km) explores and produces high spatial variability AOD maps (for instance a suburban setting).

As validation analysis over the Brazilian Northeast, we compared these MODIS-based products and MERRA2 against AERONET AOD from two sites, (Petrolina/PE and Natal/RN cities), for the period between 2015 and 2018. Petrolina is located in NEB largest Caatinga biome, while Natal is a coastal city in the Atlantic Forest biome.

The AOD seasonality from all satellite and MERRA2 products over each biome in the NEB were compared. The satellite validation analysis against AERONET showed that the AOD retrievals MxD_DB are the best products over Petrolina. The DB algorithm was developed with the main focus on bright surfaces, such as deserts, and fits well the conditions of the Caatinga as it is a brighter surface than the other biomes. Considering that, we can conclude that this product is the most adequate to use for studies in the Caatinga region. However, in the coastal region of Natal, the results from the DB algorithm are not reliable due to the low number of valid pixels with the highest QA. This is because the DB algorithm does not retrieve AOD over ocean surfaces and assigns lower QA values to pixels in the transition zones between land and ocean. As expected, the coastline also influenced the proportion of high-QA and valid pixels across all MODIS products. Compared to the Petrolina site, the percentage of high-QA pixels relative to all valid pixels at the Natal site was significantly lower. Among the MODIS products, MxD_DT are the best performer in this region. The MAIAC products generally underperform compared to Dark Target, and while the ensemble products could offer potential, the sample size is too small for definitive conclusions. A bigger sample could provide deeper insights. MERRA2 also provides good results for both AERONET sites, showing that the AOD database can be used for future studies. MERRA2's disadvantage is related to the considerably lower spatial resolution compared to the MODIS products. On average, Terra and Aqua have similar results at the Petrolina site. The good performance of DB products in Caatinga region, indicates that a regionally customized assimilation of MODIS AOD products by MERRA2 can improve its AOD analysis.

The analyses of the different biomes show that in all of them the AOD monthly average decreases during austral autumn and winter and increases in spring and summer. In general, all MODIS products agree with each other in all biomes, except the period with maximum values. DB and MAIAC yield a higher AOD in the Caatinga and Cerrado, compared to the other products. In the Atlantic Forest biome all products have similar AOD values, except for MOD_3k, which presents higher values. The Amazon biome presents the most accentuated variation throughout the year and the highest AOD. This is caused mostly by the forest fire season. All products also show differences in the AOD values, even though with similar patterns. It should be highlighted that MAIAC and DB show very similar values in all four biomes throughout the year. DB shows the best results in comparison against AERONET in the Caatinga biome, followed by MAIAC, which is also in good agreement. Thus, MAIAC may be recommended for studies in the Caatinga region, especially since it is produced on a high spatial resolution of 1 km.

The annual AOD cycle in the NEB region closely aligns with forest

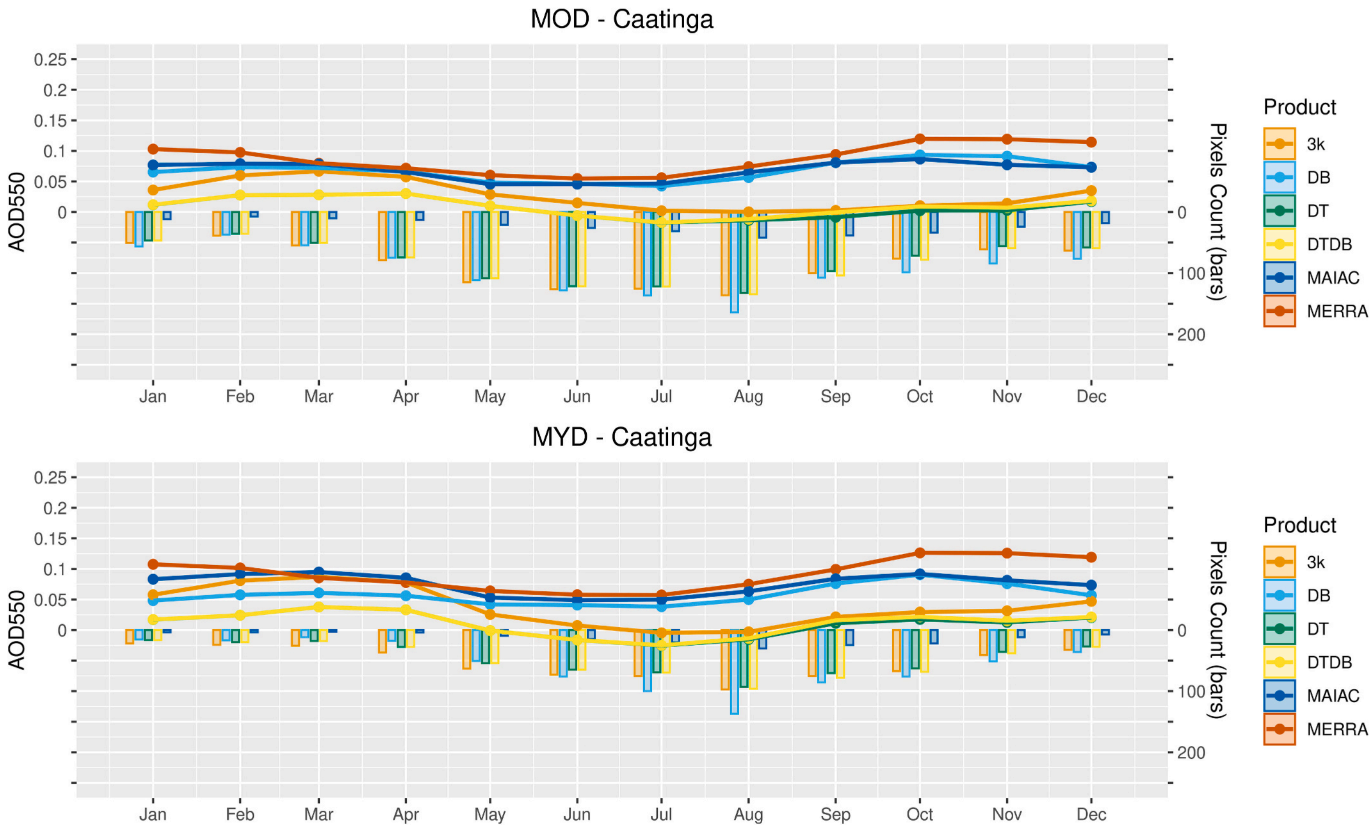

Fig. 14. Seasonal pattern of AOD550 monthly means (lines), and number of pixels (bars) in the NEB domain of the Caatinga biome from 2015 to 2018 for Terra (MOD) and Aqua (MYD) satellites products. There are scale factors in the pixel count scale of 10^3 (DT, DB, DTDB), 10^4 (3 k) and 10^6 (MAIAC). (For interpretation of the references to colour in this figure legend, the reader is referred to the web version of this article.)

fire activity, highlighting the significant contribution of local fires to the total aerosol load in the atmospheric column. The AOD data based on DT algorithm shows stronger agreement with fire activity in the Amazon region and its surroundings, while the data from DB algorithm aligns more closely with fire activity in the Caatinga. This reinforces the need for a more sophisticate selection of the AOD products tailored to regional characteristics.

Declaration of generative AI and AI-assisted technologies in the writing process

During the preparation of this work the author(s) used ChatGPT in order to improve language and readability. After using this tool/service, the author(s) reviewed and edited the content as needed and take(s) full responsibility for the content of the publication.

CRediT authorship contribution statement

Gabriel Bonow Münchow: Writing – review & editing, Writing – original draft, Visualization, Software, Methodology, Investigation, Formal analysis, Data curation, Conceptualization. **Aline Macedo de Oliveira:** Writing – review & editing, Visualization, Conceptualization. **Ediclê De Souza Fernandes Duarte:** Writing – review & editing, Validation, Conceptualization. **Daniel Camilo Fortunato dos Santos Oliveira:** Writing – review & editing, Visualization, Data curation, Conceptualization. **Bárbara Marinho Araujo:** Data curation. **Nilton Manuel Évora do Rosário:** Writing – review & editing, Writing – original draft, Supervision, Methodology, Investigation, Conceptualization. **Judith Johanna Hoelzemann:** Writing – review & editing, Writing – original draft, Supervision, Methodology, Investigation, Conceptualization.

Declaration of competing interest

The authors declare that they have no known competing financial interests or personal relationships that could have appeared to influence the work reported in this paper.

Acknowledgments

This work is a direct contribution to the research themes of the National Institute for Science and Technology - INCT Klimapolis (https://www.klimapolis.net/inct-klimapolis), which is funded by the Brazilian Ministry of Science, Technology, and Innovation (MCTI), National Council for Scientific and Technological Development (CNPq) under project number 406728/2022-4, as well as the initial German Brazilian Klimapolis Laboratory (klimapolis.net), funded by the German Federal Ministry of Education and Research (BMBF). The authors also thank the Spanish Ministry of Science and Innovation (grant no. PID2019-103886RB-I00).

Data availability

All data are publicly available

References

Albrecht, B.A., 1989. Aerosols, cloud microphysics and fractional cloudiness. Science 1979 (245), 1227–1230.
Alpopi, C., Colesca, S., 2010. Urban air quality. A comparative study of major European capitals. Theoretic. Emp. Res. Urban Manag. 5, 92–107.
Altaratz, O., Koren, I., Remer, L.A., Hirsch, E., 2014. Review: Cloud invigoration by aerosols-Coupling between microphysics and dynamics. Atmos. Res. 140–141, 38–60. https://doi.org/10.1016/j.atmosres.2014.01.009.

Arias, P.A., Bellouin, N., Coppola, E., Jones, R.G., Krinner, G., Marotzke, J., Naik, V., Palmer, M.D., Plattne, G.-K., Rogelj, J., Rojas, M., Sillmann, J., Storelvmo, T., Thorne, P.W., Trewin, B., Achuta Rao, K., Adhikary, B., Allan, R.P., Armour, K., Bala, G., Barimalala, R., Berger, S., Canadell, J.G., Cassou, C., Cherchi, A., Collins, W., Collins, W.D., Connors, S.L., Corti, S., Cruz, F., Dentener, F.J., Dereczynski, C., Di Luca, A., Diongue Niang, A., Doblas-Reyes, F.J., Dosio, A., Douville, H., Engelbrecht, F., Eyring, V., Fischer, E., Forster, P., Fox-Kemper, B., Fuglestvedt, J.S., Fyfe, J.C., Gillett, N.P., Goldfarb, L., Gorodetskaya, I., Gutierrez, J. M., Hamdi, R., Hawkins, E., Hewitt, H.T., Hope, P., Islam, A.S., Jones, C., Kaufman, D.S., Kopp, R.E., Kosaka, Y., Kossin, J., Krakovska, S., Lee, J.-Y., Li, J., Mauritsen, T., Maycock, T.K., Meinshausen, M., Min, S.-K., Monteiro, P.M.S., Ngo-Duc, T., Otto, F., Pinto, I., Pirani, A., Raghavan, K., Ranasinghe, R., Ruane, A.C., Ruiz, L., Sallée, J.-B., Samset, B.H., Sathyendranath, S., Seneviratne, S.I., Sörensson, A.A., Szopa, S., Takayabu, I., Treguier, A.-M., van den Hurk, B., Vautard, R., von Schuckmann, K., Zaehle, S., Zhang, X., Zickfeld, K., 2021. Technical Summary. In: Masson-Delmotte, V., Zhai, P., Pirani, A., Connors, S.L., Péan, C., Berger, S., Caud, N., Chen, Y., Goldfarb, L., Gomis, M.I., Huang, M., Leitzell, K., Lonnoy, E., Matthews, J.B.R., Maycock, T.K., Waterfield, T., Yelekçi, O., Yu, R., Zhou, B. (Eds.), Climate Change 2021: The Physical Science Basis. Contribution of Working Group I to the Sixth Assessment Report of the Intergovernmental Panel on Climate Change. Cambridge University Press.

Barnes, W.L., Pagano, T.S., Salomonson, V.V., 1998. Prelaunch characteristics of the Moderate Resolution Imaging Spectroradiometer (MODIS) on EOS-AM1. IEEE Trans. Geosci. Remote Sens. 36, 1088–1100. https://doi.org/10.1109/36.700993.

Buchard, V., Randles, C.A., da Silva, A.M., Darmenov, A., Colarco, P.R., Govindaraju, R., Ferrare, R., Hair, J., Beyersdorf, A.J., Ziemba, L.D., Yu, H., 2017. The MERRA-2 aerosol reanalysis, 1980 onward. Part II: Evaluation and case studies. J. Clim. 30, 6851–6872. https://doi.org/10.1175/JCLI-D-16-0613.1.

Caúla, R.H., Oliveira-Júnior, J.F., Lyra, G.B., Delgado, R.C., Heilbron Filho, P.F.L., 2015. Overview of fire foci causes and locations in Brazil based on meteorological satellite data from 1998 to 2011. Environ. Earth Sci. 74, 1497–1508. https://doi.org/10.1007/s12665-015-4142-z.

Chen, Q.X., Han, X.L., Gu, Y., Yuan, Y., Jiang, J.H., Yang, X.B., Liou, K.N., Tan, H.P., 2022. Evaluation of MODIS, MISR, and VIIRS daily level-3 aerosol optical depth products over land. Atmos. Res. 265, 105810. https://doi.org/10.1016/J.ATMOSRES.2021.105810.

Choi, M., Lim, H., Kim, J., Lee, S., Eck, T.T., Holben, B.B., Garay, M.J., Hyer, E.E., Saide, P.P., Liu, H., 2019. Validation, comparison, and integration of GOCI, AHI, MODIS, MISR, and VIIRS aerosol optical depth over East Asia during the 2016 KORUS-AQ campaign. Atmos. Meas. Tech. 12, 4619–4641. https://doi.org/10.5194/AMT-12-4619-2019.

Correia Filho, W.L.F., De Oliveira-Júnior, J.F., de Santiago, D.B., Terassi, P.M.D.B., Teodoro, P.E., De Gois, G., Blanco, C.J.C., de Souza, P.H.A., da Costa, M.S., Gomes, H.B., dos Santos, P.J., 2019. Rainfall variability in the Brazilian northeast biomes and their interactions with meteorological systems and ENSO via CHELSA product. Big Earth Data 3, 315–337. https://doi.org/10.1080/20964471.2019.1692298.

da Lopes, F.J.S., 2011. Validação dos dados do satélite CALIPSO utilizando um sistema lidar de retroespalhamento elástico e o fotômetro solar da rede AERONET. Universidade de São Paulo, São Paulo. https://doi.org/10.11606/T.85.2011.tde-28092011-103209.

da Silva, J.L.B., de Moura, G.B.A., da Silva, M.V., de Oliveira-Júnior, J.F., da Jardim, A. M.R.F., Refati, D.C., da Lima, R.C.C., de Carvalho, A.A., Ferreira, M.B., de Brito, J.I. B., de Guedes, R.V.S., Lopes, P.M.O., Nóbrega, R.S., Pandorfi, H., Bezerra, A.C., Batista, P.H.D., de Jesus, F.L.F., Sanches, A.C., Santos, R.C., 2023. Environmental degradation of vegetation cover and water bodies in the semiarid region of the Brazilian Northeast via cloud geoprocessing techniques applied to orbital data. J. S. Am. Earth Sci. 121, 104164. https://doi.org/10.1016/J.JSAMES.2022.104164.

de Andrade, M.F., Kumar, P., de Freitas, E.D., Ynoue, R.Y., Martins, J., Martins, L.D., Nogueira, T., Perez-Martinez, P., de Miranda, R.M., Albuquerque, T., Gonçalves, F.L. T., Oyama, B., Zhang, Y., 2017. Air quality in the megacity of São Paulo: Evolution over the last 30 years and future perspectives. Atmos. Environ. 159, 66–82. https://doi.org/10.1016/j.atmosenv.2017.03.051.

de Castanho, A.D.A., Martins, J.V., Artaxo, P., 2008. MODIS Aerosol Optical Depth Retrievals with high spatial resolution over an Urban Area using the critical Reflectance. J. Geophys. Res. 113, D02201. https://doi.org/10.1029/2007JD008751.

de Cavalcanti, I.F.A., Ferreira, N.J., da Dias, M.A.F.S., da Silva, M.G.A.J., 2009. Tempo e clima no Brasil. Oficina de Textos.

de INMET, I.N.M., 2018. Normais Climatológicas do Brasil (1981–2010) – Direção Predominante do Vento (Pontos cardeais e colaterais).

de Oliveira, A.M., Souza, C.T., de Oliveira, N.P.M., Melo, A.K.S., Lopes, F.J.S., Landulfo, E., Elbern, H., Hoelzemann, J.J., 2019. Analysis of atmospheric aerosol optical properties in the Northeast Brazilian atmosphere with remote sensing data from MODIS and CALIOP/CALIPSO satellites, AERONET photometers and a ground-based lidar. Atmosphere (Basel) 10. https://doi.org/10.3390/atmos10100594.

de Oliveira-Júnior, J.F., Shah, M., Abbas, A., Correia Filho, W.L.F., da Silva Junior, C.A., de Santiago, D.B., Teodoro, P.E., Mendes, D., de Souza, A., Aviv-Sharon, E., Silveira, V.R., Pimentel, L.C.G., da Silva, E.B., Haq, M.A., Khan, I., Mohamed, A., Attia, E.A., 2022. Spatiotemporal analysis of fire foci and environmental degradation in the biomes of Northeastern Brazil. Sustainability (Switzerland) 14. https://doi.org/10.3390/su14116935.

do Rosário, N.É., Sena, E.T., Yamasoe, M.A., 2022. South American 2020 regional smoke plume: intercomparison with previous years, impact on solar radiation, and the role of Pantanal biomass burning season. Atmos. Chem. Phys. 22, 15021–15033. https://doi.org/10.5194/acp-22-15021-2022.

dos Oliveira, D.C.F.S., Montilla-Rosero, E., da Lopes, F.J.S., Morais, F.G., Landulfo, E., Hoelzemann, J.J., 2021. Aerosol properties in the atmosphere of Natal/Brazil measured by an AERONET Sun-photometer. Environ. Sci. Pollut. Res. 28, 9806–9823. https://doi.org/10.1007/s11356-020-11373-z/Published.

dos Reis, J.S., Gonçalves, W.A., Mendes, D., 2021. Climatology of the dynamic and thermodynamic features of upper tropospheric cyclonic vortices in Northeast Brazil. Clim. Dyn. 57, 3413–3431. https://doi.org/10.1007/s00382-021-05873-y.

Dubovik, O., King, M.D., 2000. A flexible inversion algorithm for retrieval of aerosol optical properties from Sun and sky radiance measurements. J. Geophys. Res. Atmos. 105, 20673–20696. https://doi.org/10.1029/2000JD900282.

Eck, T.F., Holben, B.N., Reid, J.S., Dubovik, O., Smirnov, A., O'Neill, N.T., Slutsker, I., Kinne, S., 1999. Wavelength dependence of the optical depth of biomass burning, urban, and desert dust aerosols. J. Geophys. Res. Atmos. 104, 31333–31349. https://doi.org/10.1029/1999JD900923.

Ferreira, A.L., Tsai, D., Sousa, H., 2022. RECOMENDAÇÕES PARA A EXPANSÃO E A CONTINUIDADE. In: DAS REDES DE MONITORAMENTO DA QUALIDADE DO AR NO BRASIL. Pinheiros, Brazil.

Formenti, P., Rajot, J.L., Desboeufs, K., Caquineau, S., Chevaillier, S., Nava, S., Gaudichet, A., Journet, E., Triquet, S., Alfaro, S., Chiari, M., Haywood, J., Coe, H., Highwood, E., 2008. Regional variability of the composition of mineral dust from western Africa: results from the AMMA SOP0/DABEX and DODO field campaigns. J. Geophys. Res. 113, D00C13. https://doi.org/10.1029/2008JD009903.

Freund, R.J., Wilson, W.J., 2003. Statistical Methods, 2º. ed. Academic Press. https://doi.org/10.1016/C2009-0-20216-9.

Gelaro, R., McCarty, W., Suárez, M.J., Todling, R., Molod, A., Takacs, L., Randles, C.A., Darmenov, A., Bosilovich, M.G., Reichle, R., Wargan, K., Coy, L., Cullather, R., Draper, C., Akella, S., Buchard, V., Conaty, A., da Silva, A.M., Gu, W., Kim, G.-K., Koster, R., Lucchesi, R., Merkova, D., Nielsen, J.E., Partyka, G., Pawson, S., Putman, W., Rienecker, M., Schubert, S.D., Sienkiewicz, M., Zhao, B., 2017. The modern-era retrospective analysis for research and applications, Version 2 (MERRA-2). J. Clim. 30, 5419–5454. https://doi.org/10.1175/JCLI-D-16-0758.1.

Giles, D.M., Sinyuk, A., Sorokin, M.G., Schafer, J.S., Smirnov, A., Slutsker, I., Eck, T.F., Holben, B.N., Lewis, J.R., Campbell, J.R., Welton, E.J., Korkin, S.V., Lyapustin, A.I., 2019. Advancements in the Aerosol Robotic Network (AERONET) Version 3 database – automated near-real-time quality control algorithm with improved cloud screening for Sun photometer aerosol optical depth (AOD) measurements. Atmos. Meas. Tech. 12, 169–209. https://doi.org/10.5194/amt-12-169-2019.

Gupta, P., Remer, L.A., Levy, R.C., Mattoo, S., 2018. Validation of MODIS 3km land aerosol optical depth from NASA's EOS Terra and Aqua missions. Atmos. Meas. Tech. 11, 3145–3159. https://doi.org/10.5194/amt-11-3145-2018.

Holben, B.N., Eck, T.F., Slutsker, I., Tanré, D., Buis, J.P., Setzer, A., Vermote, E., Reagan, J.A., Kaufman, Y.J., Nakajima, T., Lavenu, F., Jankowiak, I., Smirnov, A., 1998. AERONET- A Federated Instrument Network and Data Archive for Aerosol Characterizationtion. Remote Sens. Environ. 66, 1–16.

Hsu, N.C., Tsay, S.-C., King, M.D., Herman, J.R., 2004. Aerosol properties over bright-reflecting source regions. IEEE Trans. Geosci. Remote Sens. 42, 557–569. https://doi.org/10.1109/TGRS.2004.824067.

Hsu, N.C., Tsay, S.-C., King, M.D., Herman, J.R., 2006. Deep blue retrievals of Asian aerosol properties during ACE-Asia. IEEE Trans. Geosci. Remote Sens. 44, 3180–3195. https://doi.org/10.1109/TGRS.2006.879540.

Hsu, N.C., Jeong, M.-J., Bettenhausen, C., Sayer, A.M., Hansell, R., Seftor, C.S., Huang, J., Tsay, S.-C., 2013. Enhanced Deep Blue aerosol retrieval algorithm: the second generation. J. Geophys. Res. Atmos. 118, 9296–9315. https://doi.org/10.1002/jgrd.50712.

Hsu, N.C., Lee, J., Sayer, A.M., Kim, W., Bettenhausen, C., Tsay, S.-C., 2019. VIIRS deep blue aerosol products over land: extending the EOS long-term aerosol data records. J. Geophys. Res. Atmos. 124, 4026–4053. https://doi.org/10.1029/2018JD029688.

IBGE, 2023. Censo Demográfico 2022 do Instituto Brasileiro de Geografia e Estatística [WWW Document]. https://sidra.ibge.gov.br/. URL https://sidra.ibge.gov.br/pesquisa/censo-demografico/demografico-2022/primeiros-resultados-populacao-e-domicilios (accessed 3.6.23).

IBGE - Instituto Brasileiro de Geografia e Estatística, 2019. Biomas e Sistema Costeiro-Marinho do Brasil [WWW Document]. In: Biomas e Sistema Costeiro-Marinho do Brasil - 1:250 000. URL https://www.ibge.gov.br/geociencias/cartas-e-mapas/informacoes-ambientais/15842-biomas.html?=&t=acesso-ao-produto (accessed 5.31.22).

Ignotti, E., de Souza Hacon, S., Leite Junger, W., Mourão, D., Longo, K., Freitas, S., Artaxo, P., Ponce, Carlos Monteiro, de Leon, A., 2010. Air pollution and hospital admissions for respiratory diseases in the subequatorial Amazon: a time series approach. Cad. Saúde Pública 26, 747–761.

Jethva, H., Torres, O., Yoshida, Y., 2019. Accuracy assessment of MODIS land aerosol optical thickness algorithms using AERONET measurements over North America. Atmos. Meas. Tech. 12, 4291–4307. https://doi.org/10.5194/AMT-12-4291-2019.

Jiang, J., Liu, J., Jiao, D., Zha, Y., Cao, S., 2023. Evaluation of MODIS DT, DB, and MAIAC aerosol products over different land cover types in the Yangtze River Delta of China. Remote Sens. 15. https://doi.org/10.3390/RS15010275. Page 275 15, 275.

Kaufman, Y.J., Koren, I., 2006a. Smoke and pollution aerosol effect on cloud cover. Science 1979 (313), 655–658. https://doi.org/10.1126/science.1126232.

Kaufman, Y.J., Koren, I., 2006b. Smoke and pollution aerosol effect on cloud cover. Science 1979 (313), 655–658. https://doi.org/10.1126/science.1126232.

Kaufman, Y.J., Tanri, D., Remer, L.A., Vermote, E.F., Chq, A., Holbenl, B.N., 1997. Operational remote sensing of tropospheric aerosol over land from EOS moderate resolution imaging spectroradiometer. J. Geophys. Res. 102, 17051–17067.

Kayanoi, M.T., Andreoli, R.V., de Cavalcanti, I.F.A., Ferreira, N.J., da Dias, M.A.F.S., 2009. Clima na Região Nordeste do Brasil. In: da Silva, M.G.A.J. (Ed.), Tempo e Clima No Brasil. Oficina de Textos, São Paulo, pp. 213–233.

Kodama, Y., 1992. Large-Scale Common Features of Subtropical Precipitation zones (the Baiu Frontal Zone, the SPCZ, and the SACZ) part I: Characteristics of Subtropical Frontal Zones. J. Meteorol. Soc. Japan. Ser. II 70, 813–836. https://doi.org/10.2151/JMSJ1965.70.4_813.

Koren, I., Martins, V.J., Remer, L.A., Afargan, H., 2008. Smoke Invigoration Versus Inhibition of Clouds over the Amazon. Science 1979 (321), 946–949. https://doi.org/10.1126/science.1159185.

Kousky, V.E., 1979. Frontal Influences on Northeast Brazil. Mon. Weather Rev. 107, 1140–1153. https://doi.org/10.1175/1520-0493(1979)107<1140:FIONB>2.0.CO;2.

Kousky, V.E., 1980. Diurnal Rainfall Variation in Northeast Brazil. Mon. Weather Rev. 108, 488–498. https://doi.org/10.1175/1520-0493(1980)108.

Kousky, V.E., Gan, M.A., 1981. Upper tropospheric cyclonic vortices in the tropical South Atlantic. Tellus 33, 538–551. https://doi.org/10.1111/J.2153-3490.1981.TB01780.X.

Landulfo, E., Lopes, F.J.S., Montilla, E., Guedes, A.G., Hoelzemann, J.J., Fernandez, J.H., Alados-Arboledas, L., Guerrero-Rascado, J.L., 2016. DUSTER lidar: transatlantic transport of aerosol particles from the Sahara and other sources: first results from the recently installed lidar and sunphotometer in Natal/Brazil. In: Lidar Technologies, Techniques, and Measurements for Atmospheric Remote Sensing XII. SPIE, p. 1000607. https://doi.org/10.1117/12.2241386.

Levy, R., Remer, L., Tanré, D., Kaufman, Y., Ichoku, C., Holben, B., Livingston, J., Russell, P., Maring, H., 2003. Evaluation of the MODIS retrievals of dust aerosol over the ocean during PRIDE. J. Geophys. Res. 108. https://doi.org/10.1029/2002JD002460.

Levy, R.C., Remer, L.A., Kleidman, R.G., Mattoo, S., Ichoku, C., Kahn, R., Eck, T.F., 2010. Global evaluation of the Collection 5 MODIS dark-target aerosol products over land. Atmos. Chem. Phys. 10, 10399–10420. https://doi.org/10.5194/acp-10-10399-2010.

Levy, R.C., Mattoo, S., Munchak, L.A., Remer, L.A., Sayer, A.M., Patadia, F., Hsu, N.C., 2013. The Collection 6 MODIS aerosol products over land and ocean. Atmos. Meas. Tech. 6, 2989–3034. https://doi.org/10.5194/amt-6-2989-2013.

Levy, R., Hsu, C., et al., 2015. MODIS atmosphere L2 aerosol product. In: NASA MODIS Adaptive Processing System. Goddard Space Flight Center.

Li, C., Lau, A.K.-H., Mao, J., Chu, D.A., 2005. Retrieval, validation, and application of the 1-km aerosol optical depth from MODIS measurements over Hong Kong. IEEE Trans. Geosci. Remote Sens. 43, 2650–2658. https://doi.org/10.1109/TGRS.2005.856627.

Li, Z., Zhao, X., Kahn, R., Mishchenko, M., Remer, L., Lee, K.-H., Wang, M., Laszlo, I., Nakajima, T., Maring, H., 2009. Uncertainties in satellite remote sensing of aerosols and impact on monitoring its long-term trend: a review and perspective. Ann. Geophys. 27, 2755–2770. https://doi.org/10.5194/angeo-27-2755-2009.

Lyapustin, A., Martonchik, J., Wang, Y., Laszlo, I., Korkin, S., 2011a. Multiangle implementation of atmospheric correction (MAIAC): 1. Radiative transfer basis and look-up tables. J. Geophys. Res. 116, D03210. https://doi.org/10.1029/2010JD014985.

Lyapustin, A., Wang, Y., Laszlo, I., Kahn, R., Korkin, S., Remer, L., Levy, R., Reid, J.S., 2011b. Multiangle implementation of atmospheric correction (MAIAC): 2. Aerosol algorithm. J. Geophys. Res. 116, D03211. https://doi.org/10.1029/2010JD014986.

Lyapustin, A., Korkin, S., Wang, Y., Quayle, B., Laszlo, I., 2012a. Discrimination of biomass burning smoke and clouds in MAIAC algorithm. Atmos. Chem. Phys. 12, 9679–9686. https://doi.org/10.5194/acp-12-9679-2012.

Lyapustin, A., Wang, Y., Laszlo, I., Hilker, T., Hall, F.G., Sellers, P.J., Tucker, C.J., Korkin, S.V., 2012b. Multi-angle implementation of atmospheric correction for MODIS (MAIAC): 3. Atmospheric correction. Remote Sens Environ 127, 385–393. https://doi.org/10.1016/j.rse.2012.09.002.

Lyapustin, A., Wang, Y., Korkin, S., Huang, D., 2018. MODIS Collection 6 MAIAC algorithm. Atmos. Meas. Tech. 11, 5741–5765. https://doi.org/10.5194/amt-11-5741-2018.

Marlier, M.E., Bonilla, E.X., Mickley, L.J., 2020. How do Brazilian fires affect air pollution and public health? Geohealth 4, e2020GH000331. https://doi.org/10.1029/2020GH000331.

Martins, V.S., Lyapustin, A., de Carvalho, L.A.S., Barbosa, C.C.F., Novo, E.M.L.M., 2017. Validation of high-resolution MAIAC aerosol product over South America. J. Geophys. Res. Atmos. 122, 7537–7559. https://doi.org/10.1002/2016JD026301.

Martins, L.D., Hallak, R., Alves, R.C., de Almeida, D.S., Squizzato, R., Moreira, C.A.B., Beal, A., da Silva, I., Rudke, A., Martins, J.A., 2018. Long-range transport of aerosols from biomass burning over southeastern South America and their implications on air quality. Aerosol Air Qual. Res. 18, 1734–1745. https://doi.org/10.4209/aaqr.2017.11.0545.

Millman, A., Tang, D., Perera, F.P., 2008. Air pollution threatens the health of children in China. Pediatrics 122, 620–628. https://doi.org/10.1542/peds.2007-3143.

Molina, M.J., Molina, L.T., 2004. Megacities and atmospheric pollution. J. Air Waste Manage. Assoc. 54, 644–680. https://doi.org/10.1080/10473289.2004.10470936.

Nguyen, T.T.N., Pham, H.V., Lasko, K., Bui, M.T., Laffly, D., Jourdan, A., Bui, H.Q., 2019. Spatiotemporal analysis of ground and satellite-based aerosol for air quality assessment in the Southeast Asia region. Environ. Pollut. 255, 113106. https://doi.org/10.1016/J.ENVPOL.2019.113106.

Oliveira, P.T., Santos e Silva, C.M., Lima, K.C., 2017. Climatology and trend analysis of extreme precipitation in subregions of Northeast Brazil. Theor. Appl. Climatol. 130, 77–90. https://doi.org/10.1007/s00704-016-1865-z.

Paredes-Trejo, F.J., Barbosa, H.A., Kumar, T.V.L., 2017. Validating CHIRPS-based satellite precipitation estimates in Northeast Brazil. J. Arid Environ. 139, 26–40. https://doi.org/10.1016/J.JARIDENV.2016.12.009.

Parrish, D.D., Singh, H.B., Molina, L., Madronich, S., 2011. Air quality progress in North American megacities: a review. Atmos. Environ. 45, 7015–7025. https://doi.org/10.1016/j.atmosenv.2011.09.039.

Randles, C.A., da Silva, A.M., Buchard, V., Colarco, P.R., Darmenov, A., Govindaraju, R., Smirnov, A., Holben, B., Ferrare, R., Hair, J., Shinozuka, Y., Flynn, C.J., 2017. The MERRA-2 aerosol reanalysis, 1980 onward. part I: System description and data assimilation evaluation. J. Clim. 30, 6823–6850. https://doi.org/10.1175/JCLI-D-16-0609.1.

Remer, L.A., Kaufman, Y.J., Tanré, D., Mattoo, S., Chu, D.A., Martins, J.V., Li, R.-R., Ichoku, C., Levy, R.C., Kleidman, R.G., Eck, T.F., Vermote, E., Holben, B.N., 2005. The MODIS aerosol algorithm, products, and validation. J. Atmos. Sci. 62, 947–973. https://doi.org/10.1175/JAS3385.1.

Remer, L.A., Mattoo, S., Levy, R.C., Munchak, L.A., 2013. MODIS 3 km aerosol product: algorithm and global perspective. Atmos. Meas. Tech. 6, 1829–1844. https://doi.org/10.5194/amt-6-1829-2013.

Remer, L.A., Levy, R.C., Mattoo, S., Tanré, D., Gupta, P., Shi, Y., Sawyer, V., Munchak, L.A., Zhou, Y., Kim, M., Ichoku, C., Patadia, F., Li, R.R., Gassó, S., Kleidman, R.G., Holben, B.N., 2020. The dark target algorithm for observing the global aerosol system: past, present, and future. Remote Sens. 12. https://doi.org/10.3390/RS12182900.

Rosário, N.E., Longo, K.M., Freitas, S.R., Yamasoe, M.A., Fonseca, R.M., 2013. Modeling the South American regional smoke plume: aerosol optical depth variability and surface shortwave flux perturbation. Atmos. Chem. Phys. 13, 2923–2938. https://doi.org/10.5194/acp-13-2923-2013.

Rudke, A.P., Martins, J.A., Martins, L.D., Vieira, C.L.Z., Li, L., Assunção da Silva, C.F., dos Santos, A.M., Koutrakis, P., de Almeida Albuquerque, T.T., 2023. Evaluation and comparison of MODIS aerosol optical depth retrieval algorithms over Brazil. Atmos. Environ. 314. https://doi.org/10.1016/j.atmosenv.2023.120130.

Sayer, A.M., Hsu, N.C., Bettenhausen, C., Ahmad, Z., Holben, B.N., Smirnov, A., Thomas, G.E., Zhang, J., 2012. SeaWiFS Ocean Aerosol Retrieval (SOAR): Algorithm, validation, and comparison with other data sets. J. Geophys. Res. Atmos. 117, n/a–n/a. https://doi.org/10.1029/2011JD016599.

Sayer, A.M., Hsu, N.C., Bettenhausen, C., Jeong, M.J., 2013. Validation and uncertainty estimates for MODIS Collection 6 "deep Blue" aerosol data. J. Geophys. Res. Atmos. 118, 7864–7872. https://doi.org/10.1002/jgrd.50600.

Sayer, A.M., Munchak, L.A., Hsu, N.C., Levy, R.C., Bettenhausen, C., Jeong, M.-J., 2014. MODIS Collection 6 aerosol products: Comparison between Aqua's e-Deep Blue, Dark Target, and "merged" data sets, and usage recommendations. J. Geophys. Res. Atmos. 119. https://doi.org/10.1002/2014JD022453, 13, 913–965, 989.

Sayer, A.M., Hsu, N.C., Bettenhausen, C., 2015a. Implications of MODIS bow-tie distortion on aerosol optical depth retrievals, and techniques for mitigation. Atmos. Meas. Tech. 8, 5277–5288. https://doi.org/10.5194/amt-8-5277-2015.

Sayer, A.M., Hsu, N.C., Bettenhausen, C., Jeong, M.J., Meister, G., 2015b. Effect of MODIS terra radiometric calibration improvements on Collection 6 deep blue aerosol products: Validation and terra/aqua consistency. J. Geophys. Res. 120. https://doi.org/10.1002/2015JD023878, 12,157-12,174.

Sayer, A.M., Hsu, N.C., Lee, J., Kim, W.V., Dubovik, O., Dutcher, S.T., Huang, D., Litvinov, P., Lyapustin, A., Tackett, J.L., Winker, D.M., 2018. Validation of SOAR VIIRS over-water aerosol retrievals and context within the global satellite aerosol data record. J. Geophys. Res. Atmos. 123. https://doi.org/10.1029/2018JD029465.

Sinyuk, A., Holben, B.N., Eck, T.F., Giles, D.M., Slutsker, I., Korkin, S., Schafer, J.S., Smirnov, A., Sorokin, M., Lyapustin, A., 2020. The AERONET Version 3 aerosol retrieval algorithm, associated uncertainties and comparisons to Version 2. Atmos. Meas. Tech. 13, 3375–3411. https://doi.org/10.5194/amt-13-3375-2020.

Souza, C.M., Shimbo, Z., Rosa, M.R., Parente, L.L., Alencar, A., Rudorff, B.F.T., Hasenack, H., Matsumoto, M., Ferreira, L., Souza-Filho, P.W.M., de Oliveira, S.W., Rocha, W.F., Fonseca, A.V., Marques, C.B., Diniz, C.G., Costa, D., Monteiro, D., Rosa, E.R., Vélez-Martin, E., Weber, E.J., Lenti, F.E.B., Paternost, F.F., Pareyn, F.G.C., Siqueira, J.V., Viera, J.L., Neto, L.C.F., Saraiva, M.M., Sales, M.H., Salgado, M.P.G., Vasconcelos, R., Galano, S., Mesquita, V.V., Azevedo, T., 2020. Reconstructing three decades of land use and land cover changes in Brazilian biomes with landsat archive and earth engine. Remote Sens. 12, 2735. https://doi.org/10.3390/rs12172735.

Tanre, D., Kaufman, Y., Herman, M., Mattoo, S., 1997. Remote sensing of aerosol properties over oceans using the MODIS/EOS spectral radiances. J. Geophys. Res.-Atmos. 102, 16971–16988. https://doi.org/10.1029/96JD03437.

Tsamalis, C., Chédin, A., Pelon, J., Capelle, V., 2013. The seasonal vertical distribution of the Saharan Air Layer and its modulation by the wind. Atmos. Chem. Phys. 13, 11235–11257. https://doi.org/10.5194/acp-13-11235-2013.

Twomey, S., 1977. The Influence of Pollution on the Shortwave Albedo of Clouds. J. Atmos. Sci. 34, 1149–1152.

Uvo, C.R.B., 1989. A zona de convergência Intertropical (ZCIT) e sua relação com a precipitação da Região Norte do Nordeste Brasileiro (Dissertação de mestrado). Instituto Nacional de Pesquisas Espaciais, São José dos Campos, SP.

Wang, Y., Lyapustin, A., 2007. The Impacts of Bowtie Effect and View Angle Discontinuity on MODIS Swath Data Gridding. Greenbelt, MD. https://ntrs.nasa.gov/api/citations/20080045515/downloads/20080045515.pdf.

Wang, Y., Wang, J., Levy, R.C., Shi, Y.R., Mattoo, S., Reid, J.S., 2021. First retrieval of AOD at fine resolution over shallow and turbid coastal waters from MODIS. Geophys. Res. Lett. 48. https://doi.org/10.1029/2021GL094344.

Weinzierl, B., Sauer, D., Esselborn, M., Petzold, A., Veira, A., Rose, M., Mund, S., Wirth, M., Ansmann, A., Tesche, M., Gross, S., Freudenthaler, V., 2011. Microphysical and optical properties of dust and tropical biomass burning aerosol layers in the Cape Verde region—an overview of the airborne in situ and lidar measurements during SAMUM-2. Tellus Ser. B Chem. Phys. Meteorol. 63, 589. https://doi.org/10.1111/j.1600-0889.2011.00566.x.

Wilks, D.S., 2019. Statistical Methods in the Atmospheric Sciences, 4a ed. Elservier, Cambridge, MA.

Witek, M.L., Garay, M.J., Diner, D.J., Smirnov, A., 2013. Aerosol optical depths over oceans: a view from MISR retrievals and collocated MAN and AERONET in situ observations. J. Geophys. Res. Atmos. 118. https://doi.org/10.1002/2013JD020393, 12,620-12,633.

Wolfe, R.E., Roy, D.P., Vermote, E., 1998. MODIS land data storage, gridding, and compositing methodology: Level 2 grid. IEEE Trans. Geosci. Remote Sens. 36, 1324–1338. https://doi.org/10.1109/36.701082.

Zhao, T.X.-P., Laszlo, I., Guo, W., Heidinger, A., Cao, C., Jelenak, A., Tarpley, D., Sullivan, J., 2008. Study of long-term trend in aerosol optical thickness observed from operational AVHRR satellite instrument. J. Geophys. Res. 113, D07201. https://doi.org/10.1029/2007JD009061.